Effect of Annealing on Structural, Optical and Electrical Properties of $(Zn_{1-x}Mg_x)_3N_2$ Thin Films

By

Iqra Elahi

(339-FBAS/MSPHY/S15)

Department of Physics

Faculty of Basic and Applied Sciences

International Islamic University, Islamabad

(2018)

(K)

530.41 MS

IQE

1 - Optical and Electrical Properties

2 - Solids - Electric Properties

3 - Layer Structure

Effect of Annealing on Structural, Optical and Electrical Properties of $(Zn_{1-x}Mg_x)_3N_2$ Thin Films

By

Iqra Elahi

(339-FBAS/MSPHY/S15)

Supervisor:

Dr. Shaista Shahzada

Associate Professor,

Department of Physics, FBAS, IIUI

Co-Supervisor:

Dr. Arshad Mehmood

DCS, NILOP

Department of Physics

Faculty of Basic and Applied Sciences

International Islamic University, Islamabad

(2018)

Effect of Annealing on Structural, Optical and Electrical Properties of $(Zn_{1-x}Mg_x)_3N_2$ Thin Films

By

Iqra Elahi

(339-FBAS/MSPHY/S15)

Thesis submitted to

Department of Physics

For the award of the degree of

MS Physics

Dr. Shaista Shahzada
Chairperson
Department of Physics (FC, FBAS)
International Islamic University
Islamabad

(Chairperson, Department of Physics)

(Dean FBAS, IIUI, Islamabad)

Department of Physics Faculty of Basic and Applied Sciences

International Islamic University, Islamabad

Department of Physics

Date: January 22, 2018,

Final Approval

It is certified that the work present in this thesis entitled "Effect of Annealing on Structural, Optical and Electrical Properties of $(Zn_{1-x}Mg_x)_3N_2$ Thin Films" by **Iqra Elahi**, Registration No. **339-FBAS/MSPHY/S15** is of sufficient standard in scope and quality for the award of degree of MS Physics from International Islamic University, Islamabad.

Committee

External Examiner

Dr Shafqat Karim

Principal Scientist, PINSTECH

Internal Examiner

Dr. Wiqar Hussain Shah

Associare Professor

Depertment of Physics, IIUI

Supervisor

Dr Shaista Shahzada

Associate Professor

Chairperson

Department of Physics

International Islamic University Islamabad

Co- Supervisor

Dr. Arshad Mehmood

DCS, NILOP

Thesis submitted to

Department of Physics

International Islamic University Islamabad

as a partial fulfillment for the award of the degree of

MS Physics

Declaration

I hereby declare that the investigation presented in this thesis work has been carried out by me. The work is original and has not been submitted earlier as a whole or in part for a degree/diploma at this or any other Institution/University.

I also declare that I do understand the term 'copyright' and 'plagiarism' and that in case of any copyright violation found in this work, I will be held fully responsible of the consequences of any such violation.

Iqra Elahi

(339-FBAS/MSPhy/S-15)

(a) Thermal Evaporation

Thermal evaporation involves heating a source inside a high vacuum chamber with produced temperature. The source is converted into steam clouds inside the chamber. The clouds moves in chamber and strike the substrate, attached to it as thin film. Thermal evaporation process has wide range of applications such as used in optical coating, wear resistance coating of surfaces, corrosion resistance coating of surfaces, high-temperature resistive coating, decorative coating, microelectronics, and solar cells.

(b) Electron Beam

Electron Beam is a form of physical vapor deposition in which a target anode is bombarded with an electron beam given off by a charged tungsten filament under high vacuum. The electron beam causes atoms from the target to transform into the gaseous phase. These atoms then precipitate into solid form, coating everything in the vacuum chamber with a thin layer of the anode material. The high melting point materials are evaporated by electron-beam evaporation because simple resistive heating cannot evaporate high melting point materials. Electron beam evaporation is a commonly used process for coating lenses and filters with anti-reflection, scratch-resistant or other specialized coatings. The process is also commonly used for coating insulating and resistor films on electronic components. The electron beam evaporation process typically involves the following components

1.3.2.2.2 Sputtering

In the sputtering method, the material enters into vacuum chamber with introducing inert gas. The inert gas is hit the material and knock out the electron and deposit on the substrate as a thin film. Sputtering is further divided into three categories (1) RF Sputtering (2) Magnetron Sputtering (3) DC Sputtering

- **RF Sputtering**

If the target is insulator then will be applied RF sputtering. The Argon atom is converted into ions. These ions bombarded with target and repelled back and sputtering process is stopped. It's polarity can be reversed by applying the radio frequency.

Declaration

I hereby declare that the investigation presented in this thesis work has been carried out by me. The work is original and has not been submitted earlier as a whole or in part for a degree/diploma at this or any other Institution/University.

I also declare that I do understand the term 'copyright' and 'plagiarism' and that in case of any copyright violation found in this work, I will be held fully responsible of the consequences of any such violation.

Iqra Elahi

(339-FBAS/MSPhy/S-15)

Certificate

It is certified that **Miss Iqra Elahi**, Registration No. **339-FBAS/MSPhy/S15** has carried out the research work related to this thesis entitled " ***Effect of Annealing on Structural, Optical and Electrical Properties of*** $(Zn_{1-x}Mg_x)_3N_2$ ***Thin Films*** " under my supervision. This work fulfills all the requirements for the award of MS Physics.

Supervisor:

Dr Shaista Shahzada

Associate Professor, IIUI

Co- Supervisor:

Dr. Arshad Mehmood

DCS, NILOP

Dedicated to;

My beloved Nana Abu, Parents

and respected teachers who supported, encouraged

and help me in all possible ways.

Acknowledgement

First of all I thank to Almighty Allah, Creator and Controller of all creations, Owner of the thoughts and creative ideas. I was not able to do anything but with the help of Allah. Best of the praises and peace be upon all the Sacred Messengers and especially for the last of them Hazrat Muhammad (Peace be upon him) and his pious who are the minarets of knowledge for all mankind.

I am very grateful to my supervisor **Dr. Shaista Shahzada** who has supported me throughout my thesis with her patience, encouragement and knowledge whilst giving me the chance to work in my own way. One simply could not wish for a better or more affectionate supervisor.

Special appreciation goes to my co. supervisor **Dr Arshad Mehmood Janjua** (DCS, NILOP)for his supervision and constant support. His invaluable help of constructive comments and suggestions throughout the experimental and results evaluation work have contributed to the success of this research. My sincere thanks go to **Dr. Mazhar Mehmood** (DCE, PIEAS) for allowing mo to use PIEAS labs. I am also thankful to **Dr Rehana Mustafa**.

I am also thankfull to **Dr.Ahmad Shuja Syed**, Engineer **Ali** and Engineer **Shoaib** of Advanced Electronics Laboratory (AEL) under IDB funded project IIUI for their help in the characterization of my samples.

I am thankful to **Miss Asma Nazir** (Ph.D scholars) at IIUI. She was always caring, kind and helping to me. I am also thankful to my friend **Eisha Butt** for her encouragement and every possible help during this research work.

I absolutely found no words to express my deepest feelings for my all .loving family members, especially to my beloved father and mother. They are always passionate, kind, supportive and encouraging. They always prayed for me. Especially my father provided me with his moral and financial support.

Iqra Elahi

IIUI, Islamabd

Table of Contents

List of Figures

Thin film deposited on p-type silicon substratre.

Thin film deposited on n-type silicon substrate.

List of Tables

List of Abbreviations

Zn_3N_2	Zinc Nitride
ZnO	Zinc Oxide
Mg_3N_2	Magnesium Nitride
MgO	Magnesium Oxide
ev	Electron Volt
nm	Nanometer
CVD	Chemical Vapour Deposition
PVD	Physical Vapour Deposition
APCVD	Atmosphere Pressure Chemical Vapor Deposition
LPCVD	Low Pressure Chemical Vapor Deposition
PECVD	Plasma Enhanced Chemical Vapor Deposition
Ar	Argon
mbar	mili bar
DC	Direct Current
RF	Radio Frequency
XRD	X-ray Diffraction
FWHM	Full Width at Half Maximum
AFM	Atomic Force Microscope
PL	Photoluminescence
UV-VIS	Ultra Violet-Visible
SE	Spectroscopic Ellipsometry

List of Symbols

Ψ	Amplitude
λ	wave length
α	Absorption coefficient
β	Full width at half maximum
σ	Conductivity
μ	Mobility
ν	Frequency
ρ	Resistivity
ω	Angular frequency
E_g	Band gap

Abstract

The thin film of Zn_3N_2 and $(Zn_{1-x}Mg_x)_3N_2$ composites deposited through DC-sputtering were annealed in air at 800°C for 2 hours. To observe the effect of annealing on structural, optical and electrical properties of thin film. It was found that the grain size of particle increase from 57.07 to 77.89 and stress reduced from 1.655×10-3 to 1.22×10^{-3}. The optical properties of thin film have been investigated by UV-Visible and Ellipsometry. The band gap of thin film slightly reduced (2.40 eV to 1.51 eV) after annealing. The electrical properties of thin film have been studied by Hall measurements and IV. The annealed thin film exhibited low carrier concentration and higher mobility than the deposited thin film.

CHAPTER 1

Introduction

1.1 Nitride semiconductors

Nitrides Semiconductors have been recognized as one of the most suitable material for optical or high-speed electronics devices due to their qualities like high band gap, electron saturation velocity and breakdown voltage [1]. Zinc nitride and Magnesium Nitride gain considerable interest due to their unique structural and optical properties such as high thermal conductivity, corrosion resistance and high temperature [2].

1.1.1 Zinc Nitride

Zn_3N_2 is a II-V compound semiconductor. Zinc nitride was first-synthesized in 1940 by Juza and Haha [1]. It has black color and its prevailing crystalline structure that of the cubic anti bixbyites. Zn_3N_2 structure is a face-centered cubic arrangement of N atoms with the large Zn atoms occupying three-fourth of the tetrahedral sites [2]. The lattice constant of Zn_3N_2 is 9.7691 A°. Numerous deposition methods have been employed to synthesis Zn_3N_2 thin film. Zn_3N_2 film has been synthesis [3, 4] by RF-magnetron sputtering, DC sputtering and molten salt chemical process. Zn_3N_2 has attracted the research interest in recent year since it can be converted into p-type ZnO:N, After oxidation at temperature higher than 400°C. It is known that the realization of reproducible and controllable p-ZnO will lead to the new area of cheap and reliable transparent optoelectronic devices. The chemical and physical property of Zn_3N_2 is studied by energy band gap, type and conductivity value. The Zn_3N_2 band gap is 1.01 to 2.12 eV [5, 6]. Band gap can be tuned depending upon technique used for deposition and characterizing of Zn_3N_2 [7, 8, 9]. Both n-type and p-type Zn_3N_2 either as-prepared and annealed form were reported [10, 11]. Zn_3N_2 is suitable as an optoelectronic material for infrared (750-1600 nm) sensor, smart window and energy conversion [12].

1.1.2 Magnesium Nitride

Mg_3N_2 is a hexagonal inorganic compound of magnesium and nitrogen. It has greenish yellow colour. Recently researcher has used various processes to prepare.

Mg_3N_2 powder with desired physical and thermal properties such as Mg direct reaction with NH_3 [13], low-pressure chemical vapor deposition method [14], and electrochemical process [15] etc. It is convenient source of Ammonia in preparation of primary amides and dihydropyridines. It has direct band gap of 1.1 to 2.5 eV [16]. Mg_3N_2 is used as catalyst to prepare some metal nitrides or non-metal nitrides. Mg_3N_2 is used to prepare cubic boron nitride (CBN) [17]. Mg_3N_2film have wide range of applications which can be used for the preparation of high hardness, high thermal conductivity, preparation of special ceramic materials, manufacture of special glass, synthesis of diamond.

1.2 Literature Review:

TingWen studied thermal annealing effect on zinc nitride thin film deposition by reactive RF-magnetron sputtering process. He observed that the optical band gap of Zn_3N_2 decrease from 1.33 to 1.14 eV after annealing. He was analyzed of film composition and suggested that concentration of oxygen increased slightly after annealing.

Voulgaropoulou et al. have reported on the deposition of Zn_3N_2 by RF-magnetron sputtering and annealing of these film in oxy gen at a temperature up to 800°C for 2h. They reported that Zn_3N_2 film had wide Band gap and annealing improved film transparency.

In 2009 H.A Mohamed studies Effect of temperature on structure and optical constant of electronic beam deposition Zn_3N_2 film at 350°C. They observed that Zn_3N_2 have direct band gap about 3.2 eV. At high temperature Zn_3N_2 film have opaque and resistive. In 2009 T.B.I vetic studied of "Effect of annealing temperature on structural and optical properties of Mg-doped ZnO".

In 2014 A.V Dyachenko et.al studies the structural properties of MgO thin film deposition by spray pyrolysis technique at different substrate temperature on glass substrate at 300 to 500°C.

In 2016 Ov.Diachankoctal studied the structure and substructure properties (identification the phase composition, lattice constant, and crystallite size of MgO) of MgO thin films at different substrate temperature.

1.3 Thin film:

A thin film, as its name implies, is a layer with a high surface-to-volume ratio. Thin film is layers of material with thickness ranging from less than 1nm to hundred of μm. The properties of thin film fluctuate from bulk material. Thin film exhibit range of biomedical and industrial applications. Important properties of thin films includes

- Thin film used of replacement parts of human body like hip joint.
- Thin films are used in eye treatment and cancer.
- Thin film used as coating of interest of protection of substrate materials against corrosion, oxidation and wear.
- Ferromagnetic thin film used in computer memory, employed in sensor, solar cell, thin film electro acoustic devices and porous nanocomposite thin film.
- Thin film used in both reflective and refractive system. Now-a-days optical lens made of multilayer of silicon oxide and silicon nitride. This lens is used in smart phone camera.

1.3.1 Steps of film deposition

Deposition of thin film depends on deposition rate, film uniformity, cost, material and substrate selection. There are three main steps involve of thin film deposition.

- Emission of particle from source.
- Movement of particle to substrate.
- Impinging of particle on substrate.

1.3.2 Deposition techniques

There are two main techniques for thin film deposition as given below.

- Chemical vapor deposition (CVD)
- Physical vapor deposition (PVD)

In physical vapor deposition, the deposited material is said to have the same composition as the source (i.e. target material) whereas chemical vapor deposition changes the composition of the film from that of the sources.

1.3.2.1 Chemical vapour deposition:

In this method, the reactant gases are filled into the reaction chamber. The chemical reaction can take place between reactant and substrate due to deposition. First CVD process were reported in 19th century and used for the development of carbon for colour pigment. There are three types of sources that can be used in CVD for manufacturing of thin film. These sources are present in the form of gases, volatile liquid or a combination of both.

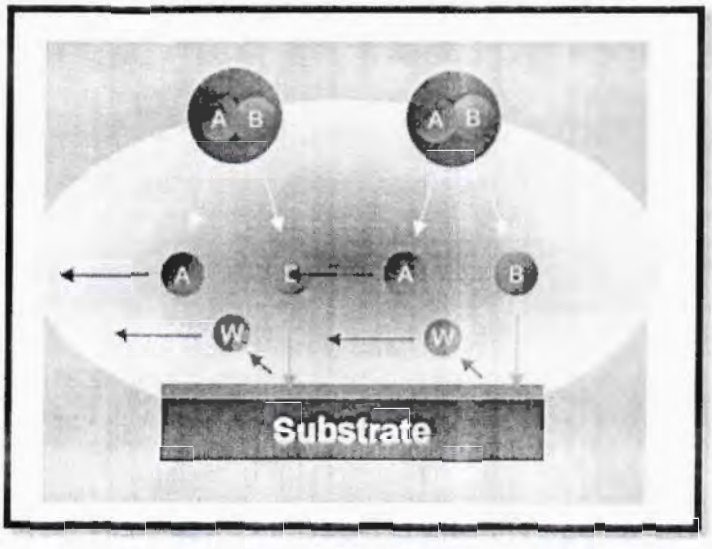

Fig 1.1: Process of Chemical Vapour Deposition (CVD)

The CVD source material must be stable at room temperature, have sufficient volatility and the reaction temperature should be less than melting point of substrate.

CVD can be classified into three types.

- Atmospheric Pressure Chemical Vapor Deposition (APCVD)
- Low Pressure Chemical Vapor Deposition (LPCVD)
- Plasma Enhanced Chemical Vapor Deposition (PECVD)

The advantages and disadvantages of these methods summarized in table no 1.1.

Table 1.1: Types of Chemical Vapour Deposition

Types	Advantages	Disadvantages	Usage	Pressure/ Temperature
APCVD	Fast, simple	Poor step coverage	Oxide and epitaxial silicon	10-100 Kpa 350-1200°C
LPCVD	Excellent, uniformity	High temperature, low deposition rate	Poly silicon, nitride oxide	100 Pa 550-600°C
PECVD	Low temperature	Risk for particle and chemical contamination	Low temperature oxides	200-600 Pa 300-400°C

1.3.2.2 Physical Vapour Deposition

In this method there is no chemical change take place. In this technique that material physically transport from a condensed phase source to a substrate like evaporation or sputtering. Physically process divided into two types (A) Evaporation (B) Sputtering

1.3.2.2.1 Evaporation

In evaporation method source material loaded in the container and applied at high temperature. Substrate fixed on top of container and material start evaporation and impinging on the surface of substrate. Evaporation further divide into two categories,(1) Thermal evaporation and (2) Electron beam.

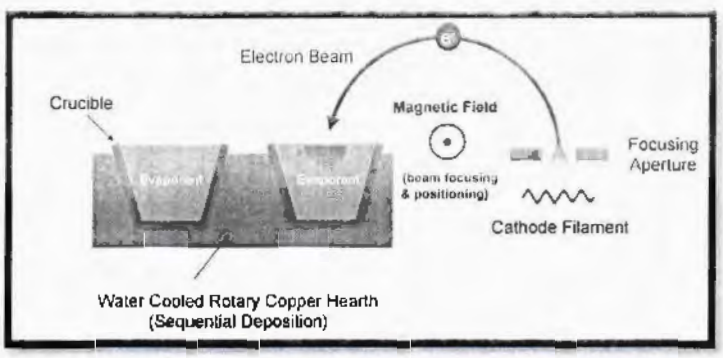

Fig 1.2: Diagram show the process of Evaporation methods

(a) Thermal Evaporation

Thermal evaporation involves heating a source inside a high vacuum chamber with produced temperature. The source is converted into steam clouds inside the chamber. The clouds moves in chamber and strike the substrate, attached to it as thin film. Thermal evaporation process has wide range of applications such as used in optical coating, wear resistance coating of surfaces, corrosion resistance coating of surfaces, high-temperature resistive coating, decorative coating, microelectronics, and solar cells.

(b) Electron Beam

Electron Beam is a form of physical vapor deposition in which a target anode is bombarded with an electron beam given off by a charged tungsten filament under high vacuum. The electron beam causes atoms from the target to transform into the gaseous phase. These atoms then precipitate into solid form, coating everything in the vacuum chamber with a thin layer of the anode material. The high melting point materials are evaporated by electron-beam evaporation because simple resistive heating cannot evaporate high melting point materials. Electron beam evaporation is a commonly used process for coating lenses and filters with anti-reflection, scratch-resistant or other specialized coatings. The process is also commonly used for coating insulating and resistor films on electronic components. The electron beam evaporation process typically involves the following components

1.3.2.2.2 Sputtering

In the sputtering method, the material enters into vacuum chamber with introducing inert gas. The inert gas is hit the material and knock out the electron and deposit on the substrate as a thin film. Sputtering is further divided into three categories (1) RF Sputtering (2) Magnetron Sputtering (3) DC Sputtering

- **RF Sputtering**

If the target is insulator then will be applied RF sputtering. The Argon atom is converted into ions. These ions bombarded with target and repelled back and sputtering process is stopped. It's polarity can be reversed by applying the radio frequency.

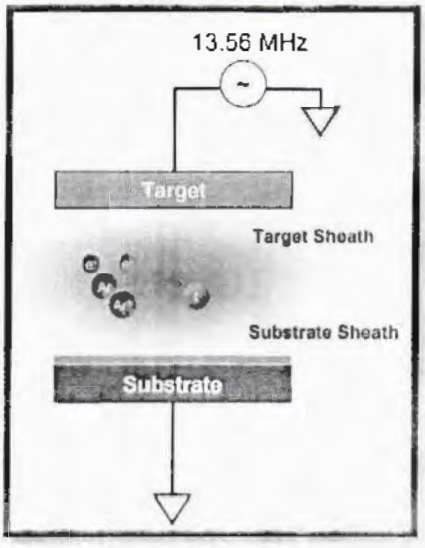

Fig 1.3: Process of Radio Frequency Sputtering

- **Magnetron Sputtering**

. Magnetron Sputtering is a Plasma Vapor Deposition (PVD) process in which plasma is created and positively charged ions from the plasma are accelerated by an electrical field superimposed on the negatively charged electrode or target. The positive ions are accelerated by potentials ranging from a few hundred to a few thousand electron volts and strike the negative electrode with sufficient force to dislodge and eject atoms from the target. These atoms will be ejected in a typical line of sight cosine distribution from the face of the target and will condense on surfaces that are placed in proximity to the magnetron sputtering cathode.

- **DC Sputtering**

Source and substrate are placed on two parallel electrodes inside a chamber filled with inert gas. DC voltage is applied to the electrode and produced free electron in chamber and accelerate by electron. Energetic free electron hit the argon atom and produced argon ions. These ions hit the source and knock out the atom from surface, they are move up and deposited on surface. DC sputtering technique can use for semiconductor. DC sputtering used for deposition of Zinc Magnesium Nitride thin film. The advantage of this technique is that low growth temperature, good adhesion of thin film on the substrate and high deposition. The main advantage of DC sputtering is that to produce economically feasible large area thin film with desired composition and properties.

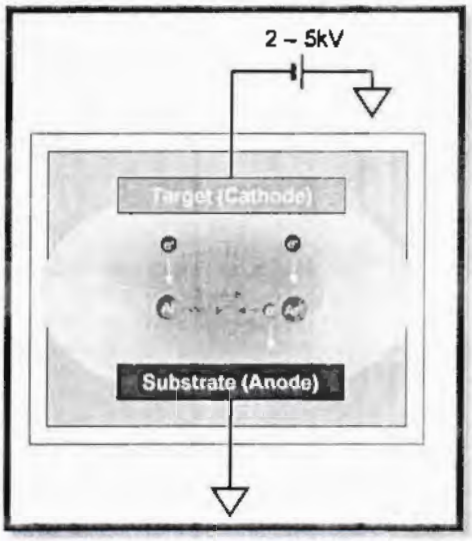

Fig 1.4: DC Sputtering

1.4 Annealing:

This process involves heat treatment in which material is heated at high temperature after cooling it slowly the particle of material will be arrange into the definite lattice. Pre-annealing thin film show amorphous behavior due to the presence of impurities, defects stress and reduced grain size. Thermal treatment is method that used to improved crystal quality, reduced defects and stress. Annealing is used to reduce band gap of material. The structural and optical properties are favorable for semiconductor devices especially for light emitted devices. The main advantage of annealing is that how the properties of the material are affected by increasing temperature. There are three main steps of annealing.

- Heating to material at desired temperature
- Holding material at that temperature
- Slowly cooling usually to room temperature

1.4.1. Types of Annealing:

There are three types of annealing (1) Full Annealing (2) Process Annealing (3) Stress Relief Annealing

1.4.1.1 Full Annealing

Heating the material to the critical point of temperature is holding there for a time period and then it cool slowly in the furnace. The range of temperature is 30°C-40°C.

1.4.1.2 Process Annealing

This heat treatment is used for softening and increase the ductility of strain hardened material. The range of temperature is 260°C-760°C.

1.4.1.3 Stress Relief Annealing

In this treatment will not change any phase of the material. This process used for recystallization, stress improved and removed defect from material. The range of temperature is 600-800°C. This type of annealing is used for improving Zinc magnesium nitride thin film because our film has the presence of stress and defects before annealing. There are three main application of stress Relief Annealing describes below.

- To obtain fine grain size
- To remove internal stress
- To improve Machinability

1.4.2. Annealing Treatment

Annealing treatment is divided in three regions, (1) Recovery (2) Recrystallization (3) Grain Growth

1.4.2.1 Recovery:

Motion, annihilation of point defect and rearrangement of dislocation of subgrain and grains boundaries are involved in this region at low temperature. In this region, no change takes place in grain structure of the material. Small change in hardness are observed during recovery that can be recognized to decrease in dislocation and point defect density.

1.4.2.1. Recrystallization:

In this region nucleation and growth of strain-free grains is deformed at high temperature. In this region grains grow, the dislocations in matrix are annihilated at boundaries of newly formed grains.

1.4.2.2. Grain Growth:

Grain growth occurs when recrystallization material is further annealed at same temperature. Large grains grow by an increase in average grain size and boundaries between annealed grains migrate.

1.4.3 Application of Annealing of thin film

- Thermal annealing is the method that used to improve crystal quality and to study structural defect of material.
- Annealing process produced a significant change of thin film that is important for electronic devices of zinc nitride.

CHAPTER 2

Experimental setup and work

2.1 DC sputtering method:

DC-Sputtering method was carried out to prepare thin films [17].This method has several advantage of low deposition rate [18]. It is suitable for producing good quality cost effective dielectric film [19]. The experiments were carried out in National Institute of Laser and Optics (NILOP). DC-Sputtering apparatus contain following components.

1. Deposition Chamber
2. DC Power Supply
3. Gas mass flow controller
4. Vacuum gauges for pressure measurement
5. Vacuum pumps

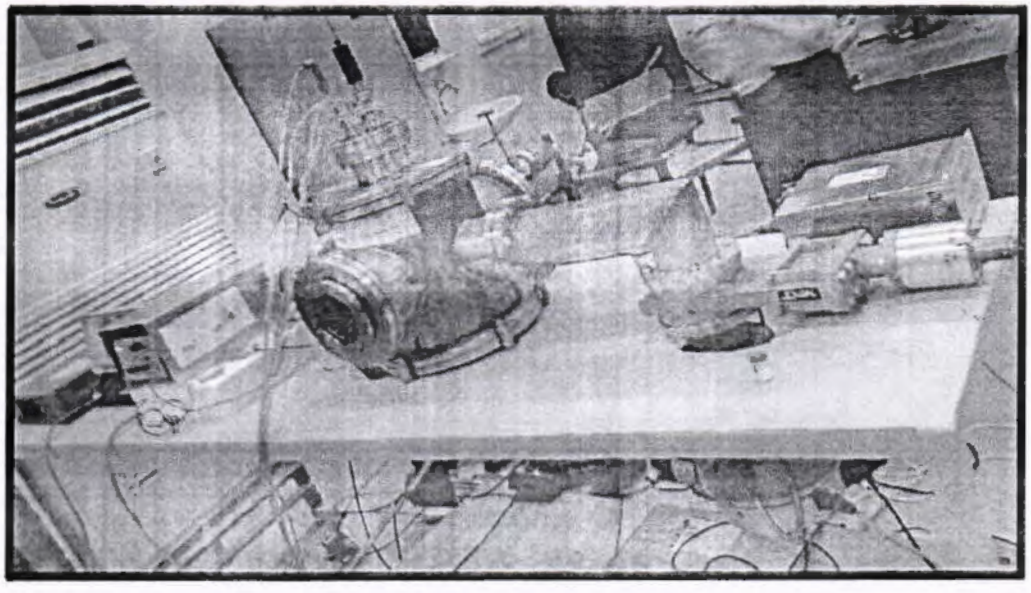

Fig 2.1: Experiment Setup of DC-Sputtering method at NILOP

2.2 Experimental procedure:

Granular zinc and magnesium were grinding with help of mortar pestle. After grinding, zinc and magnesium were weight using a physical balance at IIUI lab. Zinc and magnesium fine powder were mixed in motor pestle in different weight ratio and

make the pellet under 3 Ton pressure. All the pellets are put in furnace for sintering. The temperature of furnace raised from room temperature to 350°C. The pellets kept at that temperature for two hours. The weight ratio of samples is given below in the table.

Samples	Zn weight ratio	Mg weight ratio
Zn	28.92g	0g
ZnMg1	27.47g	1.45g
ZnMg2	24.58g	2.89g
ZnMg3	21.69g	7.23g
ZnMg4	18.8g	10.12g

Table 2.1: Samples and weight ratios

Two-inch pallet was placed in target holder. P-type silicon was put on the substrate holder. The chamber was closed and tightly fitted. The shape of the chamber was O-rings and clamps. The rotary pump was used for maintaining rough vacuum 10^{-3} mbar. The scroll pump was used to obtain vacuum 10^{-6} mbar and backing the turbo molecular pump. The electrical heater was used to attained uniform thickness of thin film that fixed under substrate holder at temperature of 300°C. 5% of nitrogen was flowed in the chamber. For plasma generation, Ar gas was used as inert gas. After plasma generation, water flow through pipes to kept apparatus cool. The deposition was held with deposition pressure 10^{-3}-10^{-4} mbar at one hour. After two-hour the chamber was cool down, then it was opened and the sample was taken out and kept in samples boxes [17].

2.3 Annealing:

After deposition of thin films, samples were annealed in the box furnace at 800°C in the air due to reducing of nitrogen concentration and the addition of oxygen.

2.3.1 Collaboration of Furnace:

- Turn on the furnace and check the temperature of furnace that should display the room temperature.
- Turn on the furnace the upper display is actual temperature and lower display is the set point pressed up and down arrow and fixed the 800°C temperature.

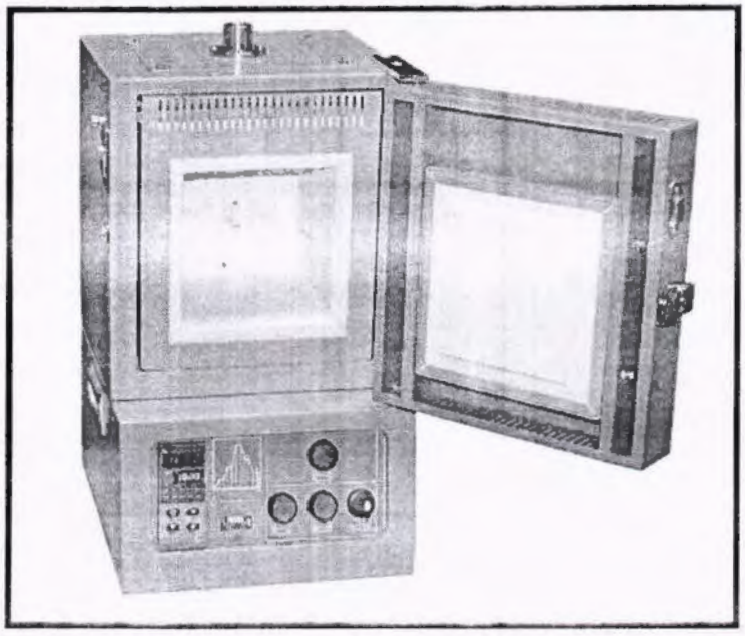

Fig 2.2: Furnace

2.3.2 Procedure:

The sample was placed in the holder and put in the center of the furnace. So that it may not touch the walls of the furnace. Sample was annealed at 800°C. The annealing process was carried out in three steps.

1. Heating at a rate of 6.66°C/min to reach 800°C for 2 hours.
2. Static annealing at 800°C for 2 hours.
3. Cooling at a rate of 6.66°C/min to reach 0°C.

Samples were taken out and stored in sample boxes. Detailed of samples is given in table 2.2.

Two beams are used in an ultraviolet spectroscopy, one is the reference beam and the other one is sample beam. The reference beam directly move to the detector without any interaction with the sample. The sample beam hits the sample revealing it to ultraviolet light of continuously changing wavelength. The intensities' ratio between sample and reference beam are recorded in detector.

Band gap:

The energy band gap has been calculated from reflectance spectra of ZnMg thin film by Kubelka-Munk function. This function gives the relationship between absorption coefficient and scattering coefficient.

$$F(R) = \frac{\alpha}{S} = \frac{(1-R)^2}{2R} \text{ ---------- (3.4)}$$

In this equation α, S *and* R represents the absorption coefficient, scattering coefficient and reflectance. The energy gap of ZnMg thin film can be calculated from the reflectance spectra using Tauc and Menth method

$$(h\nu\alpha)^m = A(h\nu - E_g) \text{ ---------- (3.5)}$$

h, v, α, m *and* A represents the Plank's constant, frequency of incident light, absorption coefficient and constants, m = 2 is used for direct band gap and ½ for indirect band gap of semiconductor.

3.6 Spectroscopy Ellipsometry:

Ellipsometry is a visual apparatus which measures the change in polarization upon reflection. It is non-contact and non-destructive technique used for the optical and structural characterization of thin films [22]. Ellipsometry is used to determine film thickness, refractive index and extinction coefficient. It has a wide use in engineering because of large possibilities to produce and create the application model for a great variety of material, including unknown combination.

Four component of Ellipsometry are light source, two polarizer, two compensators and detector. First, light from the source passes through the polarizer and gets linearly polarized. It then passes through the compensator and falls on the

thin film. The light penetrates into thin film also it will get reflected partially through compensator and analyzer polarizer. At the end it falls on detector.

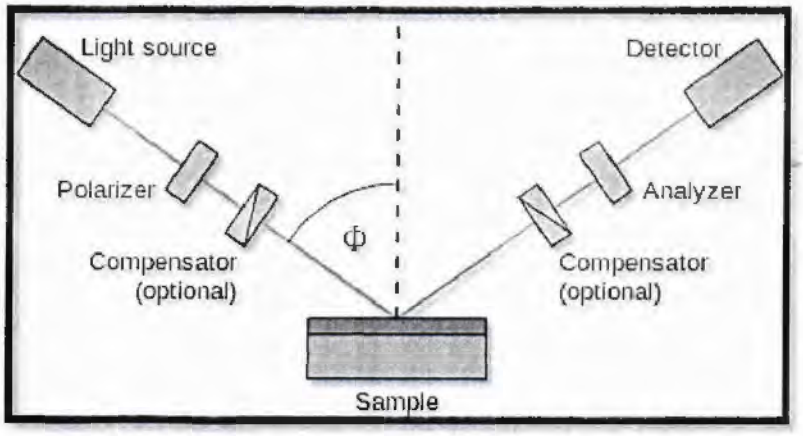

Fig 3.7: Schematic diagram of Ellipsometry.

Two values are measured by Ellipsometry Δ and Ψ. Ψ represent the amplitude of R_p and R_s for the light waves polarized p (parallel with plane of incident) and s (perpendicular on plane of incident). Δ represents the phase difference between p and s. Finally obtained results are shown in condition of phase and amplitude related as

$$tan\Psi e^{-i\Delta} = \frac{R_p}{R_s} \text{--------} 3.6$$

Ellipsometry data and its fitting were done by using Sentec SE 800 at Advanced Electronics Lab (AEL), IIUI. The band gap of data attained by SE can be calculated by using these formulae:

$$k = \frac{k\lambda}{4\pi} \text{ ---------- (3.7)}$$

$$\alpha = \frac{4\pi k}{\lambda} \text{ ---------- (3.8)}$$

3.7 Electrical characterization:

Electrical characterization is carried out to measure the resistivity, conductivity, carrier concentration and electrical mobility. Hall Effect and IV characterization techniques are used to check the electrical properties of sample.

3.7.1 Hall Effect:

Edwin Hall discovered the Hall Effect in 1847. Hall Effect explains the behavior of free charge carries in semiconductor when an electric field is applied.

Sheet resistance can be measured by two methods, first is collinear method and second is Van der Pauw method. In our case, Van der Pauw method was used for the calculation of sheet resistance. A square area is selected for probing. Resistivity and Hall coefficient can be easily measured for any sample through Van der Pauw method. The benefit of this method is that it can be used to understand the properties of any random shaped sample. The sample must be two dimensional. An error occurs at the time when sample surface is not uniform. A current is circulated in all direction and corresponding values of voltage are measured.

The equation shows the carrier concentration holes (n) and electrons (p) in term of hall coefficient (R_H) is given by

$$n = \frac{1}{qR_h} \; or \; p = \frac{1}{qR_h} \text{--------3.9}$$

Mobility equation for the electrons (μ_n) and holes (μ_p) is expressed in terms of Hall coefficient is given:

$$\mu_n = \sigma_n R_H \; or \; \mu_p = \sigma_p R_H \text{-------3.10}$$

'σ_n' and 'σ_p' represent the conductivities due to electrons and holes respectively.

CHAPTER 4

Results and Discussion

We prepared zinc magnesium nitride thin films samples (ZnMg0 (Zn=100%), ZnMg1 (Zn 95%, Mg 5%), ZnMg2 (Zn 85%, Mg 15%), ZnMg3 (Zn 75%, Mg 25%) and ZnMg4 (Zn 65%, Mg 35%)) on both n and p silicon subtrate by using reactive DC sputtering method and annealed them in air at 800°C. These thin films were characterized to observe the effect of annealing on their structural, optical as well as electrical properties. The results obtained of samples (before and after annealing) from XRD, Raman Spectroscopy, UV-Visible, PL, Ellipsometry and Electrical Characterizations are discussed briefly in the present chapter.

4.1 XRD (X-ray Diffraction):

The structural analysis of all the thin films was carried out using X-ray Diffractrometre in the range $2\theta = 10^{0}$-90^{0} (λ=0.154 nm).

4.1.1 The thin films deposited on n-type silicon substrate:

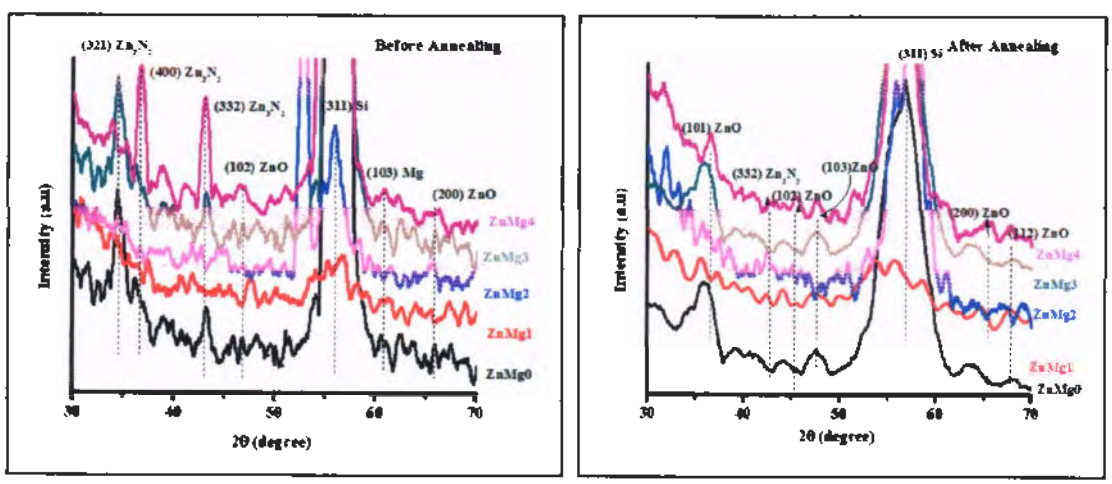

Fig 4.1: XRD spectra of zinc magnesium nitride thin films before and after annealing on n-type silicon substrate.

The XRD patterns of zinc nitride thin films (ZnMg0 (Zn=100%), ZnMg1 (Zn 95%, Mg 5%), ZnMg2 (Zn 85%, Mg 15%), ZnMg3 (Zn 75%, Mg 25%) and ZnMg4

(Zn 65%, Mg 35%)) deposited on n-type silicon substrate for as deposited and after annealing samples are given in figure 4.1. The XRD trends of thin films before annealing show noise and somewhat amorphous behavior. The peak of Zn_3N_2 (332) (JCPDS Card No. 01-1150 & 36-1451) was observed in all samples of as deposited thin films [24]. The intensity of Zinc nitride peak corresponding to (332) was very sharp and intense in sample ZnMg4 but other samples had weaker and wide peak. After Annealing, the intensity of peak Zn_3N_2 (332) got reduced and it became wide. The grain size of Zn_3N_2 (332) is also increased and reduced the strain, hence the peak shifted from higher theta value towards lower one at 800°C is shown in table no 4.1 and 4.2.

Table No 4.1: Structural parameter of ZnMg thin films before annealing deposited on n-type silicon. (ZnMg0 (Zn 100%), ZnMg1 (Zn 95%, Mg 5%), ZnMg2 (Zn 85%, Mg 15%), ZnMg (Zn 75%, Mg 25%) and ZnMg (Zn 65%, Mg 35%)).

	Material	2θ (deg.)	θ (deg.)	FWHM β		Grain size D (nm)	Micro strain ε ($x10^{-3}$)
				In deg.	In Rad ($\times10^{-3}$)		
ZnMg4	Zn_3N_2 (332)	43	21	0.15	2.61	57.07	1.656
ZnMg3	Zn_3N_2 (332)	43.15	21.5	0.04	0.69	215	0.43
ZnMg2	Zn_3N_2 (332)	42.65	21.3	0.04	0.69	215.5	0.42
ZnMg1	Zn_3N_2 (332)	42.9	21.4	0.05	0.87	171	0.55
ZnMg0	Zn_3N_2(332)	43.145	21.5	0.05	0.87	171	0.552
ZnMg4	ZnO (102)	46.77	23.3	0.04	0.69	218	0.40
ZnMg3	ZnO (102)	46.8	23.4	0.04	0.69	218	0.398
ZnMg2	ZnO (102)	46.77	23.3	0.03	0.52	290	0.301
ZnMg1	ZnO (102)	47.5	23.76	0.05	0.87	174	0.49
ZnMg0	ZnO (102)	46.84	23..42	0.04	0.697	216	0.402

The peak of ZnO (102) appeared in all the thin films of before and after annealed samples. Before annealing, the intensity of peak ZnO (102) was sharp and had a large grain size along with less strain. The intensity of peak started getting lesser and reduced with an increase in temperature. The peak of ZnO (002) has

reduced grain size and therefore increased strain after annealing. The main reason is that the phase ZnO (002) is not enhanced with temperature that is reported by [28].

Table No 4.2: Structural parameter of ZnMg thin films after annealing deposited on n-type silicon. (ZnMg0 (Zn 100%), ZnMg1 (Zn 95%, Mg 5%), ZnMg2 (Zn 85%, Mg 15%), ZnMg3 (Zn 75%, Mg 25%) and ZnMg (Zn 65%, Mg 35%))

	Material	2θ (deg.)	θ (deg.)	FWHM β		Grain size D (nm)	Micro strain ε ($x10^{-3}$)
				In deg.	In Rad ($\times10^{-3}$)		
ZnMg4	Zn_3N_2 (332)	42.6	21.32	0.11	1.91	77.89	1.22
ZnMg2	Zn_3N_2 (332)	42.40	21.2	0.12	2.09	71.12	1.34
ZnMg1	Zn_3N_2 (332)	42.25	21.125	0.3	5.23	28.4	3.384
ZnMg4	ZnO (102)	45.26	22.63	0.08	1.39	108	0.833
ZnMg3	ZnO (102)	45.52	22.76	0.12	2.09	71.9	1.245
ZnMg2	ZnO (102)	45.12	22.56	0.08	1.39	107	8.36
ZnMg1	ZnO (102)	45.47	22.73	0.28	4.88	30.79	2.91
ZnMg0	ZnO (102)	45.52	22.75	0.18	3.14	47.86	1.87

The Zn_3N_2 peaks at (321) and (400) (JCPDS No 35-762) appeared before annealing but after annealing these peaks got suppressed [27]. After annealing, the ZnO (102) JCPDS no (80-0075) peak appeared, it became apparent that unintentional oxygen adsorption had taken place, along with some kind of reaction between oxygen and the excess zinc in the thin films structure which as a result converted them into highly resistive p-type nitrogen doped ZnO films [25, 26]. The peak of Mg (103) appeared before annealing due to difference of ionic radii of magnesium and zinc. After annealing, Mg (103) peak was suppressed in all the samples of thin films. After annealing, new oxide peaks appeared at ZnO (103) and ZnO (112) in all samples of thin films due to annealing in oxygen at 800°C. With increasing the temperature, the bonds between zinc and nitrogen broke down and oxygen reacted with zinc [29].

Overall, the effect of annealing is that the structural quality of thin films got improved and defects were reduced that is further confirmed by PL results. Thin films

rearrange itself at 800°C temperature, that's why strain was reduced and grain size of particle has increased as shown in table No 4.1 and 4.2.

4.1.2 Thin films deposited on p-type silicon substrate:

The XRD pattern of zinc nitride thin films (ZnMg0 (Zn=100%), ZnMg1 (Zn 95%, Mg 5%), ZnMg2 (Zn 85%, Mg 15%), ZnMg3 (Zn 75%, Mg 25%) and ZnMg4 (Zn 65%, Mg 35%)) as deposited on p-type silicon substrate is shown in figure 4.2. The grain size and strain calculated for ZnO (102) peak in sample ZnMg4 for as deposited and after annealing are tabulated below. The results show that the grain size of ZnO is increased and strain have reduced significantly from the thin films. The intensity of ZnO (102) peak increased and sharpened after annealing. After annealing, the thin films recyrstallized itself. So, ZnO (102) peak appeared in other samples namely ZnMg3 & ZnMg2 with grain sizes 16.64 & 83.3 nm respectively. The peak (102) in ZnMg2 shifted from higher theta value to lower theta value. Hence, the grain size of ZnMg2 increased and strain have lessened as compared to those in samples ZnMg4 & ZnMg3.

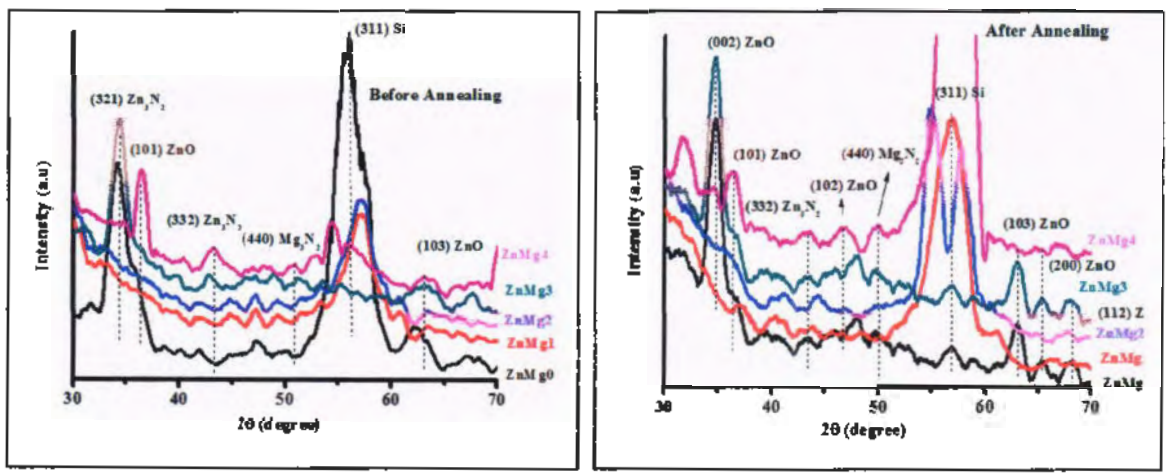

Fig 4.2: XRD spectra of zinc magnesium nitride thin films before and after annealing on p-type silicon substrate.

The Zinc nitride peak (332) appeared in ZnMg4 and ZnMg3 for as deposited and after annealed samples. After annealing, this peak also appeared in sample named ZnMg2. In ZnMg4, the grain size of peak Zn_3N_2 (332) increased and strain was reduced but in ZnMg3 decrease in grain size was observed along with increased strain.

Table No 4.3: Structural parameter of ZnMg thin films before annealing deposited on n-type silicon. (ZnMg0 (Zn 100%), ZnMg1 (Zn 95%, Mg 5%), ZnMg2 (Zn 85%, Mg 15%), ZnMg3 (Zn 75%, Mg 25%) and ZnMg (Zn 65%, Mg 35%))

	Material	2θ (deg.)	θ (deg.)	FWHM β		Grain size D (nm)	Micro strain ε ($x10^{-3}$)
				In deg.	In Rad. ($\times10^{-3}$)		
ZnMg4	ZnO (102)	34.65	17.325	0.7	12.2	11.9	9.7
ZnMg3	ZnO (102)	34.65	17.325	0.5	8.72	16.64	6.9
ZnMg2	ZnO (102)	34.45	17.225	0.1	1.74	83.3	1.40
ZnMg4	Zn_3N_2 (332)	43.35	21.65	0.1	1.74	85.7	1.09
ZnMg3	Zn_3N_2 (332)	43.4	21.7	0.2	3.48	42.8	2.186
ZnMg0	Zn_3N_2 (332)	43.45	21.675	0.1	1.74	85.7	1.09
ZnMg4	Mg_3N_2 (440)	50.45	25.225	0.1	1.74	85.7	1.09
ZnMg3	Mg_3N_2 (440)	50.11	25	0.03	1.74	88.05	0.92
ZnMg3	ZnO (103)	63	31	0.1	1.74	93.42	0.709
ZnMg0	ZnO (103)	63.1	31.55	0.1	1.74	93.42	0.709

The Mg_3N_2 (440) peak was observed in samples ZnMg4 and ZnMg3 in both before and after annealing spectra. After annealing, the grain size of the peak corresponding to Mg_3N_2 (440) had reduced and strain was increased but in sample No ZnMg4 only. Mg_3N_2 had increased grain size and reduced strain as shown in table no 4.4. This peak did not appear in other samples due to low concentration of magnesium.

The intensity of ZnO (103) was increased and widened in ZnMg3 and ZnMg4 after annealing which indicates the enhancement of crystal quality [30]. The grain size of peak ZnO (103) was observed to be increased and strain was released after annealing. Before annealing, Zn_3N_2 (321) peak appeared but after annealing this peak was vanished. On increasing temperature, the bonds between zinc and nitride broke and oxygen bonded with liberated zinc and formed ZnO (002).

Table No 4.4: Structural parameter of ZnMg thin films after annealing deposited on n-type silicon. (ZnMg0 (Zn 100%), ZnMg1 (Zn 95%, Mg 5%), ZnMg2 (Zn 85%, Mg 15%), ZnMg3 (Zn 75%, Mg 25%) and ZnMg (Zn 65%, Mg 35%))

	Material	2θ (deg.)	θ (deg.)	FWHM β		Grain size D (nm)	Micro strain ε ($x10^{-3}$)
				In deg.	In Rad. ($\times10^{-3}$)		
ZnMg4	ZnO (102)	36.44	18.22	0.88	15.3	9.53	11.62
ZnMg4	Zn_3N_2 (332)	43.2	21.6	0.4	6.97	21.3	4.40
ZnMg3	Zn_3N_2 (332)	42.8	21.4	0.1	1.74	85.5	1.10
ZnMg4	Mg_3N_2 (440)	50.8	25.4	0.08	1.30	99.7	0.731
ZnMg3	Mg_3N_2 (440)	51.14	25.57	0.3	5.23	29.37	2.73
ZnMg4	ZnO (103)	63.05	31.52	0.3	5.23	31.08	2.13
ZnMg3	ZnO (103)	63.1	31.55	0.4	6.9	23.57	2.80
ZnMg2	ZnO (103)	63.4	31.7	0.5	8.7	18.7	3.52
ZnMg1	ZnO (103)	63.4	31.7	0.5	8.7	18.7	3.52
ZnMg0	ZnO (103)	63.3	31.65	0.2	3.4	47.8	1.37

4.2 Raman Analysis:

Effects of annealing on the vibrational and rotational modes of Zinc Magnesium nitride thin films were checked by utilizing the Raman spectroscopy.

4.2.1 Thin films deposited on n-type silicon substrate:

A Raman spectra for Zinc Magnesium Nitride thin films (ZnMg0 (Zn=100%), ZnMg1 (Zn 95%, Mg 5%), ZnMg2 (Zn 85%, Mg 15%), ZnMg3 (Zn 75%, Mg 25%) and ZnMg4 (Zn 65%, Mg 35%)) deposited on n-type silicon substrate in as deposited and after annealing is shown in figure 4.3. Zn-O has four optical modes ($A_1+E_1+E_2+B_1$). A_1 and B_1 are polar, Raman and infrared modes while E_2 modes (E_2^{high} and E_2^{low}) are non polar and Raman modes [31, 32, 33]. E_2^{high} is associated with oxygen atoms and E_2^{low} is associated with Zn sub lattice. B_1 modes are silent. A_1 and E_2 split into longitudinal and transverse optical components (LO & TO). Zn-N

has two Raman Active vibration modes with respect to wavelength at 257 [34] and 565 cm^{-1} [35].

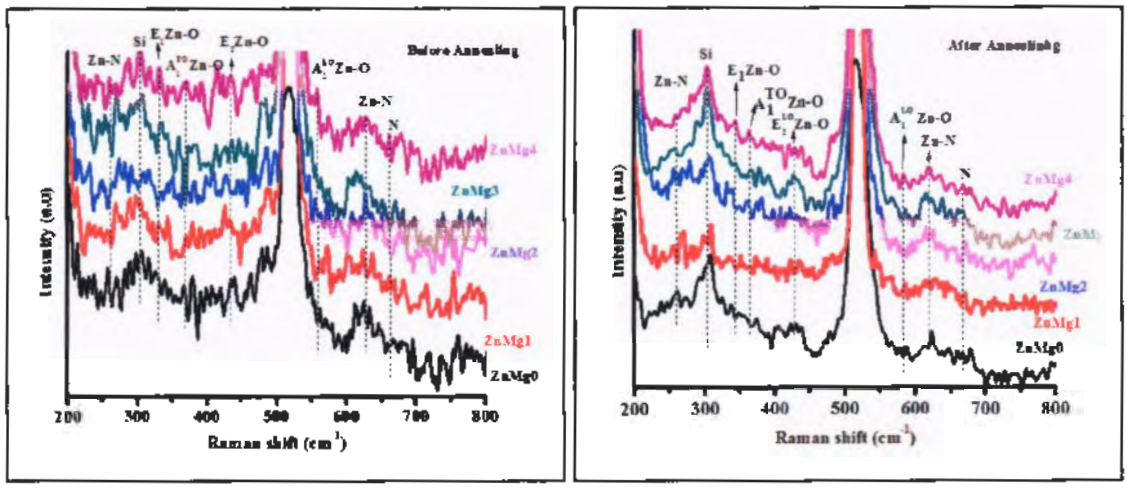

Fig 4.3: Raman spectra of zinc magnesium nitride thin films before and after annealing on n-type silicon substrate.

Before annealing, both Raman active vibrational modes of Zn-N related to bulk Raman peaks appeared at 257.8 (originally at 257 cm^{-1}) and 619 cm^{-1} (originally at 565 cm^{-1}). These peaks shifted from lower Raman no. to higher ones with blue shifts and decreased in bond length. After Annealing, Zn-N Raman modes with respect to wave lengths 260cm^{-1}& 619 cm^{-1} are suppressed in samples ZnMg4 & ZnMg3 and appeared in samples ZnMg0, ZnMg1 & ZnMg2.

The Raman scattering for the ZnO vibrational modes was dominated by two peaks at about 332 (originally at 340 cm^{-1}) and 433 cm^{-1}(originally at 430 cm^{-1}) which can be assigned to the E_1& E_2 optical phonon of ZnO crystal, and after annealing these peak were shifted at about 344 cm^{-1} with blue shift (originally at 340 cm^{-1}) & 429 cm^{-1} with red shift (originally at 430 cm^{-1}). Longitudinal and transverse optical modes of ZnO were present at 559 & 370 cm^{-1} in before annealed samples. After annealing, these modes of ZnO got shifted at 583cm^{-1}& 363 cm^{-1}. The nitrogen peak was prominent at 661 cm^{-1} before annealing. After annealing, the nitrogen peak is shifted from 661cm^{-1} to 667 cm^{-1}.

Overall, after annealing, most of the peaks shifted from low towards high Raman shift and decreased in bond length as it is already evident by XRD.

4.2.2 Thin films deposited on p-type silicon substrate:

Figure 4.4 shows the Raman spectra of Zinc magnesium nitride thin films (ZnMg0 (Zn=100%), ZnMg1 (Zn 95%, Mg 5%), ZnMg2 (Zn 85%, Mg 15%), ZnMg3 (Zn 75%, Mg 25%) and ZnMg4 (Zn 65%, Mg 35%)) for as deposited and after annealed samples. Before annealing, Raman Active vibrational modes of Zn-N were observed at 249 cm^{-1}(originally at 257 cm^{-1}) and 618 cm^{-1} (originally at 565 cm^{-1}). After annealing, these peaks were shifted from low Raman to high Raman no. at 268 cm^{-1}(originally at 257 cm^{-1}) and 619 cm^{-1} (originally at 565 cm^{-1}).

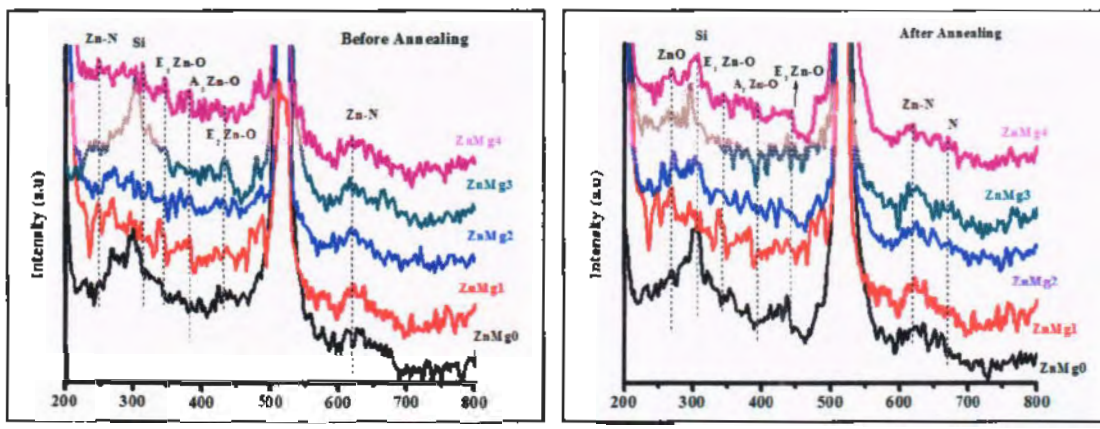

Fig 4.4: Raman spectra of zinc magnesium nitride thin films before and after annealing on p-type silicon substrate.

Two distinguishable peaks related to E_1 and E_2 Raman active mode of ZnO appearing at 344 and 382 cm^{-1} in as deposited thin films show blue shift after annealing i.e. they appear at 346 and 444 cm^{-1}.

4.3 UV Visible Spectroscopy:

Reflectance, absorption and transmission are three types of UV-VIS spectroscopy. The band gap of zinc nitride was evaluated with the help of UV-VIS reflectance.

4.3.1 Thin films deposited on n-type silicon substrate:

The reflectance spectra of the Zn_3N_2 thin films with different concentrations of Mg and Zn are shown in figure 4.5.

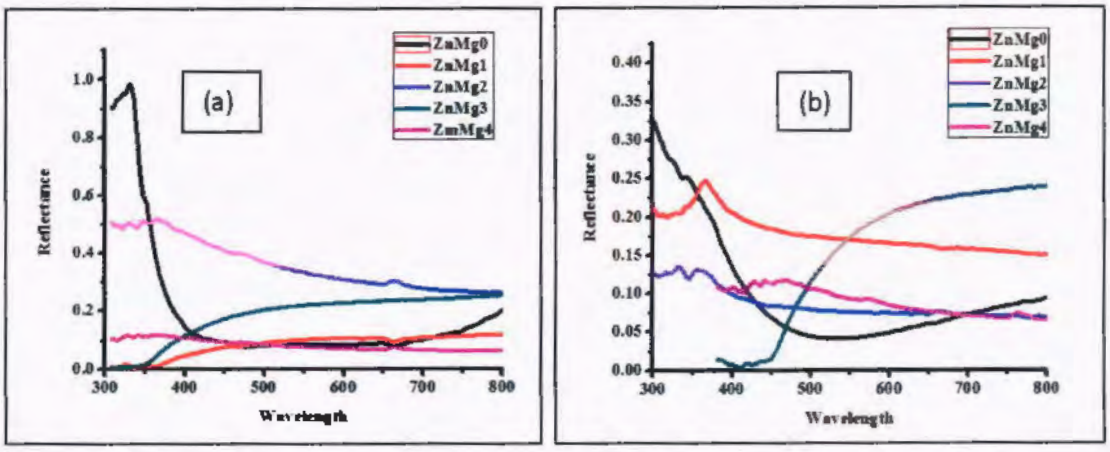

Fig 4.5: The reflectance curves of thin films (a) before and (b) after annealing.

The reflectance of ZnMg0 is decreased from 0.99 to 0.33 and wavelength is reduced from 310 to 300 nm. The reflectance of ZnMg1 and ZnMg3 increased with annealing due to increase in oxidation level.

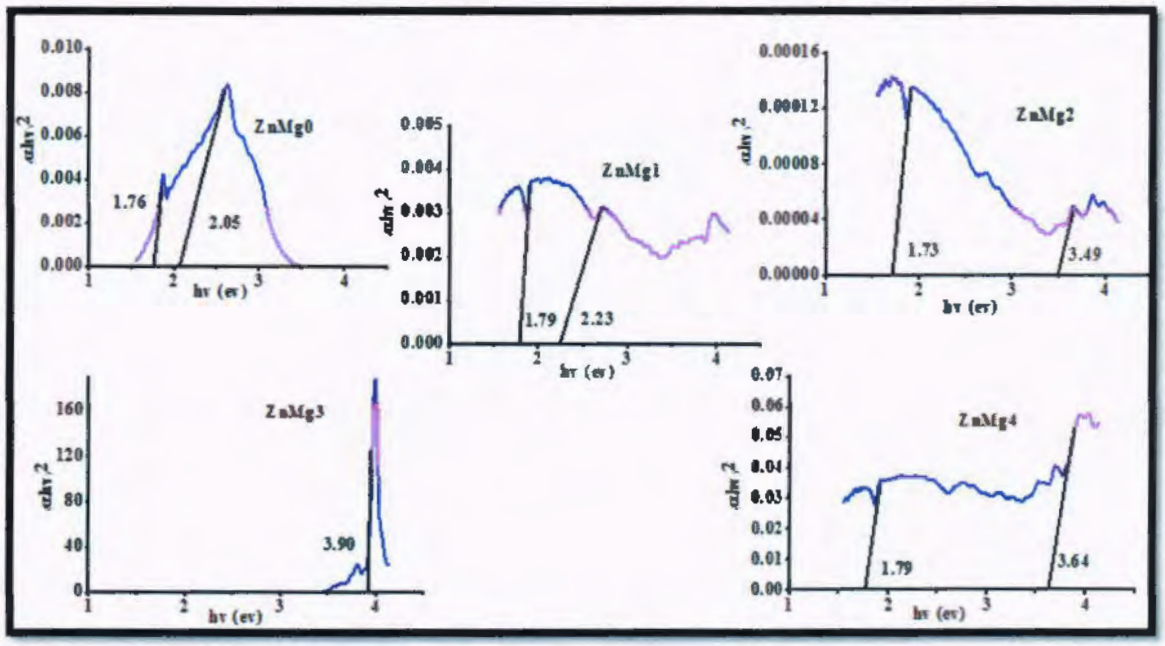

Fig 4.6: The graphs show the band gap of Zinc Magnesium nitride thin films before annealing on n-type silicon substrate.

The graphs in the figure 4.6 show the optical band gaps of Zinc magnesium nitride thin films (ZnMg0 (Zn=100%), ZnMg1 (Zn 95%, Mg 5%), ZnMg2 (Zn 85%, Mg 15%), ZnMg3 (Zn 75%, Mg 25%) and ZnMg4 (Zn 65%, Mg 35%)) calculated by the reflectance spectra by extrapolating the linear position of curve $(\alpha hv)^2$ versus hv.

Before annealing, the band gaps of pure zinc nitride thin films were observed to be 1.76 and 2.05 eV and after annealing, the band gap is reduced from 2.05 to 1.77 eV. The pure Zinc nitride thin film has no impurities added in it. Before annealing, thin films showed amorphous behavior due to vacancy defects. After annealing of thin films improved crystallinity and reduced defects were observed that's why band gap was significantly reduced after annealing.

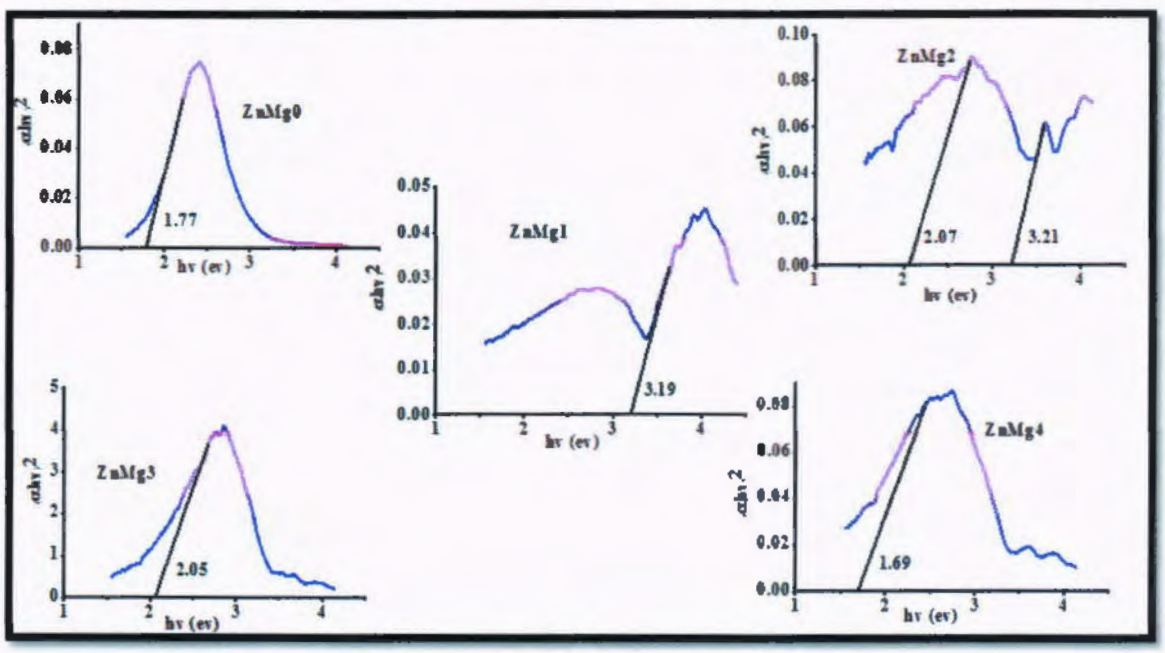

Fig 4.7: The graphs show the band gap of Zinc Magnesium nitride thin films after annealing on n-type silicon substrate.

The 5% magnesium added in target to fabricate the thin film of sample ZnMg1 which showed more reflection before annealing. Before annealing, the band gaps were 1.79, 2.32 and 3.85 eV and after annealing the band gaps were 1.75, 3.38 and 3.56 eV. In ZnMg2, graph showed more transition before annealing so the band gap was larger at 1.7, 3.49 eV and after annealing the band gap was 3.19 eV. In ZnMg3, the graph showed a uniform behavior for before annealing as compared to after annealing. In this thin film, magnesium concentration added was 25%, the thin film recrystallized itself at 800°C, and hence more defects were generated in thin film that is also confirmed by PL results. In ZnMg3, the thin film shows more expansion after annealing. The band gaps of ZnMg3 of as deposited and annealing were 3.9 and 2.05 eV. In ZnMg4 thin films showed more transition before annealing that's the reason of

the large energy band gap between valance band and conduction band. The band gaps before annealing were1.79, 3.69 eV and after annealing it is 1.69 eV.

Table No 4.5: Band gap of Zinc Magnesium Nitride thin films (deposited on n-type silicon subtrate) calculated by Tauc and Menth method.

Samples	Before Annealing E_g (ev)	After Annealing E_g (ev)
Zn_3N_2 (Zn=100%)	1.76, 2.05	1.77
ZnMg1(Zn=95%, Mg=5%)	1.79, 2.31	3.19
ZnMg2 (Zn=85%, Mg=15%)	1.73, 3.49	2.07, 3.21
ZnMg3 (Zn=75%, Mg=25%)	3.90	2.05
ZnMg4 (Zn=65%, Mg=35%)	1.79, 3.64	1.69

Overall, samples are prepared on n-type silicon substrate. There is a slight decrease in the band gap after annealing in all the samples of thin films. The band gap has reduced after annealing which implies that the oxygen filled the vacancy defect and interstitial defect [36]. By XRD, it is already proved that grain size has increased upon thermal treatment that's annealing.

4.3.2 UV-Visible Reflectance Spectroscopy p-type silicon substrate:

Reflectance, absorption and transmission are three modes of spectroscopy. The band gap of zinc nitride was examined with the help of UV-VIS reflectance. The reflectance spectra of the Zn_3N_2 thin films with different concentration are shown in figure 4.8.

It is observed that pure zinc nitride thin films exhibit highest values of reflectance i.e. from 0.18 to 0.27 with increase in annealing temperature. The wavelength also shifted from 255 nm to 282 nm. Overall the reflectance of thin films is decreased after annealing. The reflectance of ZnMg2, ZnMg3 and ZnMg4 has decreased after annealing due to the increase of concentration of magnesium. With increase of temperature, thin films rearranged themselves which resulted in reduced strain and enhanced grain sizes that have shown in XRD results.

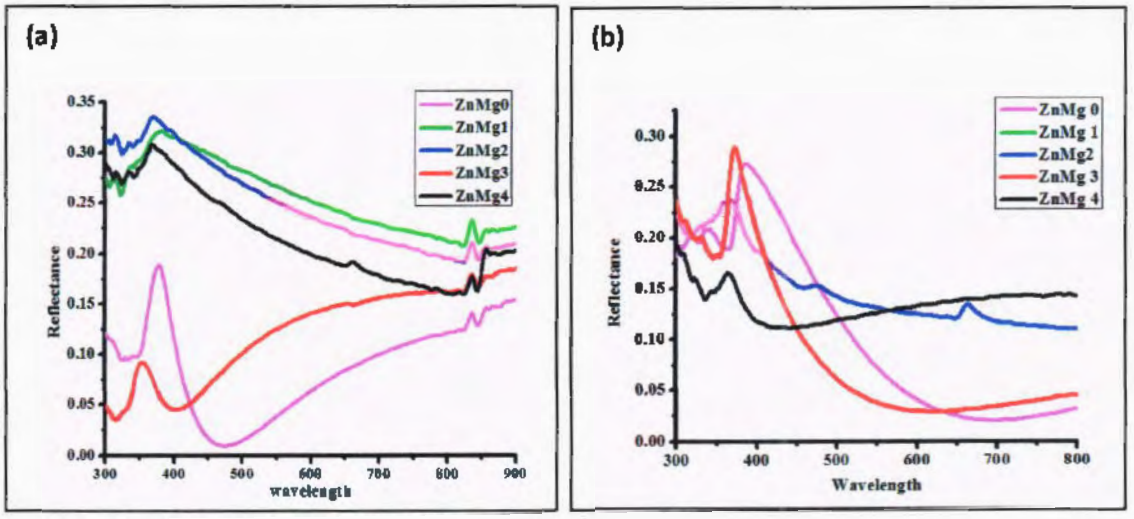

Fig 4.8: Reflectance spectra of ZnMg thin films with different Mg concentration (a) before and (b) after annealing.

It is observed that pure zinc nitride thin films exhibit highest values of reflectance i.e. from 0.18 to 0.27 with increase in annealing temperature. The wavelength also shifted from 255 nm to 282 nm. Overall the reflectance of thin films is decreased after annealing. The reflectance of ZnMg2, ZnMg3 and ZnMg4 has decreased after annealing due to the increase of concentration of magnesium. With increase of temperature, thin films rearranged themselves which resulted in reduced strain and enhanced grain sizes that have shown in XRD results.

The above graphs show that optical band gaps of Zinc Magnesium nitride thin films (ZnMg0 (Zn=100%), ZnMg1 (Zn 95%, Mg 5%), ZnMg2 (Zn 85%, Mg 15%), ZnMg3 (Zn 75%, Mg 25%) and ZnMg4 (Zn 65%, Mg 35%)) are calculated by reflectance spectra by extrapolating the linear position of curve $(\alpha h\nu)^2$ versus hv. Before annealing, the band gap of pure zinc nitride thin film (ZnMg0) is 2.40 eV due to presence of strain and small size of grains. The gap between valance band and conduction band is large so that electrons required more energy to jump from VB to CB. Due to thermal treatment, the band gap of ZnMg0 is reduced that is 1.51 eV due to increase in grain size.

In ZnMg1, before annealing thin film showed more transitions due to amorphous structure and addition of magnesium as shown in figure 4.9 (ZnMg1). The band gaps of thin film were 3.5 and 4.5 eV. Annealing in air at 800°C improved the crystallinity (that's confirmed by XRD) and therefore band gap of film is reduced

(3.27 and 3.59 eV). Before annealing, ZnMg2 showed more transition with small grain size and larger strain so that band gaps were larger i.e. 3.48, 4.3 and 4.6 eV. After annealing, the band gap (1.89 and 3.14 eV) reduced, it can also be inferred that incorporation addition of oxygen may be the reason for reduction of band gap in addition to improved crystallinity

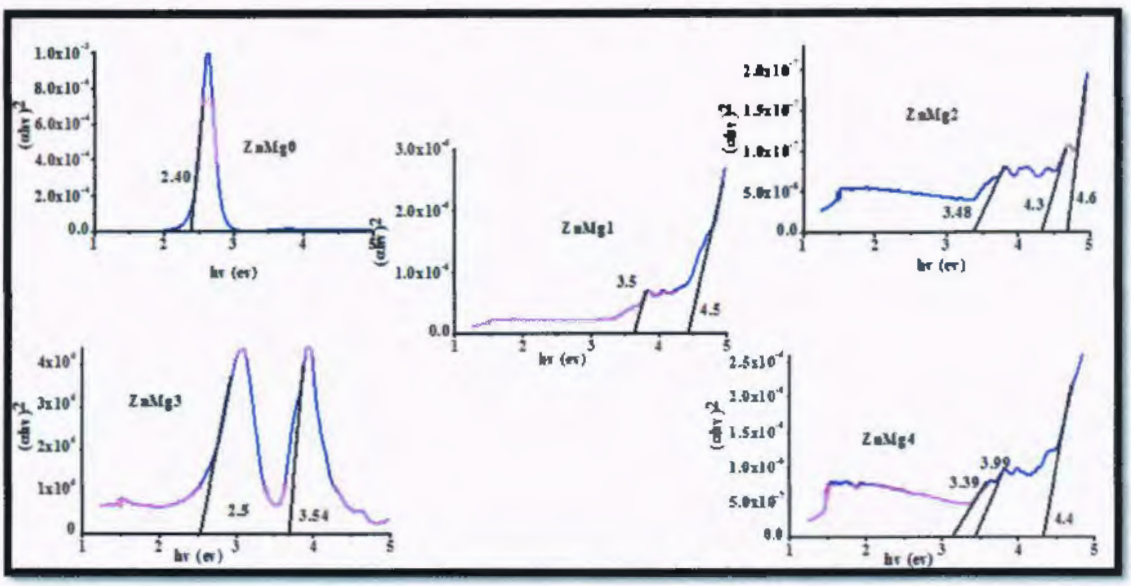

Fig 4.9: The graphs show the band gap of Zinc Magnesium nitride thin films before annealing on p-type silicon substrate.

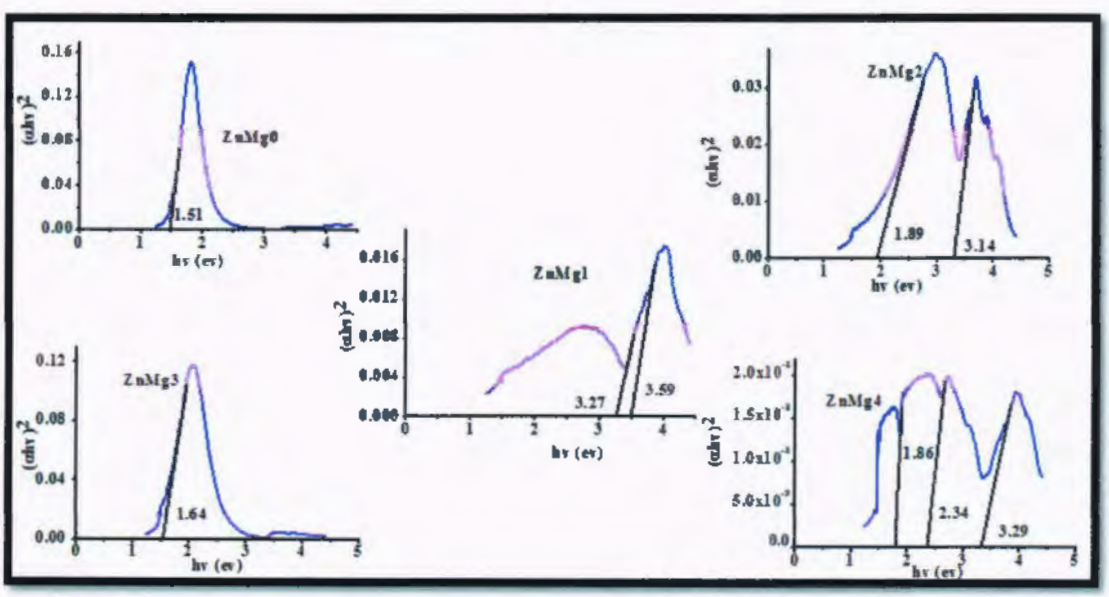

Fig 4.10: The graphs show the band gap of Zinc Magnesium nitride thin films after annealing on p-type silicon substrate.

. Before annealing, ZnMg3 has band gaps 2.5 and 3.54 eV and after annealing the band gap became 1.64 eV. In ZnMg4 before annealing, the band gaps were 3.39, 3.99 and 4.4 eV and after thermal treatment the band gaps got reduced i.e. 1.86, 2.34 and 3.29 eV.

All graphs in figure 4.10 show that after annealing, the band gaps of thin films are decreasing which proves that oxygen fills the vacancy defects and interstitial defects and this indicates that tensile strain of thin films is slightly removed. Grain size in these thin films is increased which is confirmed by XRD [37]. The change in band gap in ZnO is due to different reasons such as thermal expansion, mismatched strain, dopants and the presence of growth strain. Increased concentration of holes due to increase in oxidation temperature will be further shown in Hall measurements result [36].

Table No 4.6: Band gap of Zinc Magnesium Nitride thin films (deposited on p-type silicon subtrate) calculated by Tauc and Menth method.

Samples	Before Annealing E_g (ev)	After Annealing E_g (ev)
Zn_3N_2 (Zn=100%)	2.40	1.51
ZnMg1(Zn=95%, Mg=5%)	3.5, 4.5	3.27, 3.59
ZnMg2 (Zn=85%, Mg=15%)	3.48, 4.3, 4.6	1.89, 3.14
ZnMg3 (Zn=75%, Mg=25%)	2.5, 3.54	1.64
ZnMg4 (Zn=65%, Mg=35%)	3.39, 3.99	1.86, 2.34, 3.29

4.4 Photoluminescence Spectroscopy (PL):

The PL spectra of before and after annealed samples has been carried out to investigate the interstitial and vacancy defects present in samples. These defects are very sensitive to different parameters such as doping concentration and size of particle.

4.4.1 ZnMg thin films deposit on n-type silicon substrate:

Figure 4.11 shows the PL spectra of Zinc Magnesium Nitride thin films (ZnMg0 (Zn=100%), ZnMg1 (Zn 95%, Mg 5%), ZnMg2 (Zn 85%, Mg 15%), ZnMg3

(Zn 75%, Mg 25%) and ZnMg4 (Zn 65%, Mg 35%)) deposited on n-type silicon substrate for before and after annealing case. Before annealing, it can be seen that most of transitions take place in UV and Visible region. In UV region, small and wide peaks are observed with respect to wavelength at 357, 381 and 388 nm in all samples except ZnMg4 sample. While in ZnMg4, the intensity of peak was large and wide from wavelength 357 to 381 nm. In visible region, the peaks are observed at 416, 469, 486 and 505 nm with violet, blue and green emissions. Blue emission shows more transitions that describe vacancy defects present in thin films [38]. Green emission is due to ZnO which shows intrinsic defect states [39, 40].

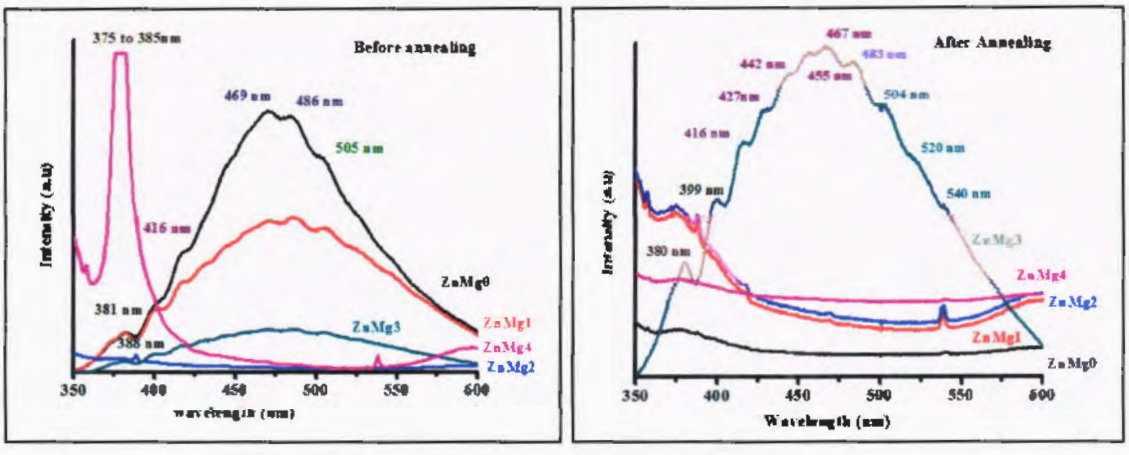

Fig 4.11: PL graph of Zinc Magnesium Nitride thin films before and after annealing on n-type silicon substrate.

After Annealing, small transitions occurred in UV region in all graphs but in visible region the trend of all graphs are smooth and did not show transitions except for ZnMg3. By increasing temperature, mostly defects are removed from thin films [38]. In case of ZnMg4, emission of band gap appeared from 400 to 500 nm in which 465 nm shows blue region that is owing to recombination of electrons with existence of oxygen vacancies [41]. These vacancies are produced by different factors such as unbalanced oxygenation during subsequential crystallization process, Mg vacancies and interstitial defects [42, 43].

4.4.2 ZnMg thin films deposit on p-type silicon substrate:

Figure 4.12 shows relationship between wavelength and intensity of thin films (ZnMg0 (Zn=100%), ZnMg1 (Zn 95%, Mg 5%), ZnMg2 (Zn 85%, Mg 15%), ZnMg3

(Zn 75%, Mg 25%) and ZnMg4 (Zn 65%, Mg 35%)) for as deposited and after annealed samples. Before annealing, small and wide peaks are observed in UV region at 381 and 398 nm while in visible region, more inter and intra band transitions take place from 416 to 504 nm. Blue and green emissions show more transitions which indicate vacancy defects present in thin films [40].

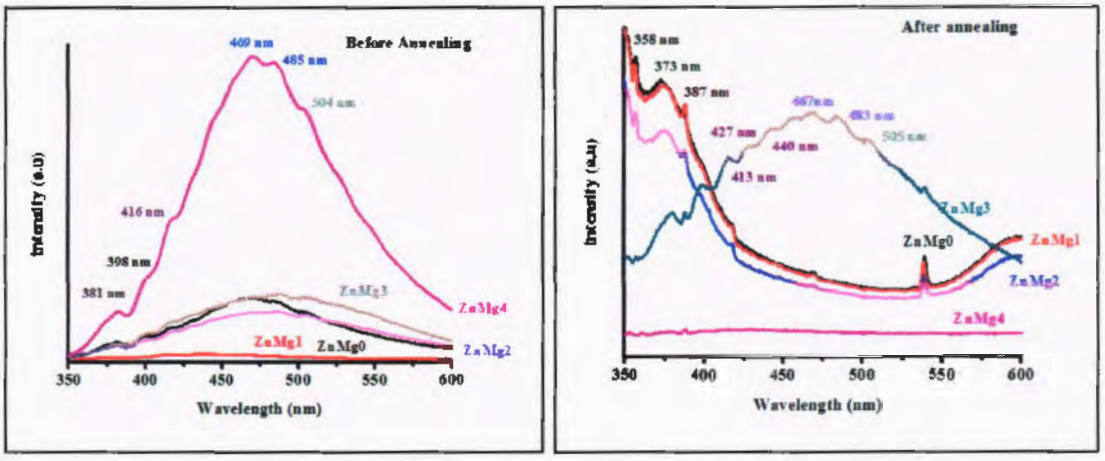

Fig 4.12: PL graph of Zinc Magnesium Nitride thin films before and after annealing on p-type silicon substrate.

After annealing, vacancy defects are mostly removed from thin film and reflection is shown at 358, 373 and 387 nm in UV region. ZnMg3 showed more reflections in visible region due to incorporation of oxygen which is confirmed by XRD spectrum [40].

4.5 Spectroscopic Ellipsometry:

The main objective of spectroscopy ellipsometry on samples was to find out the thickness of thin films that is approximately to closely original values. Refractive index, extinction coefficient, complex dielectric constant can be calculated by spectroscopic ellipsometry. Initial value of the phase and amplitude of thin films can calculate by spectroscopic ellipsometry. It can also give information uniformity, anisotropy, composition, crystallinity and surface roughness of the thin films.

4.5.1 ZnMg thin films deposited on n-type silicon substrate:

Reflection:

Reflection spectra of annealed and unannealed thin films deposited on Si wafers is shown in fig 4.13. It can be observed that there is no difference in reflection

pattern of as deposited and annealed thin films. In sample ZnMg2 reflection rises from 2.5 to 2.6 for wavelength range 300-350 nm which then gradually decreases to 1.9 in wavelength range 350-800 nm. ZnMg1 shows similar behavior as that of ZnMg2 but with smaller reflection. ZnMg4 shows small variation as compared to ZnMg1 and ZnMg2 whereas ZnMg0 and ZnMg3 show quiet different behaviors in their reflection. In the wavelength range 300-350 nm, reflection decreases to minimum value and then increases to 800 nm in ZnMg3. Whereas in ZnMg0, reflection first rises in wavelength range 300-350 nm then decreases in wavelength range 350-370 nm and again rises beyond 370 nm.

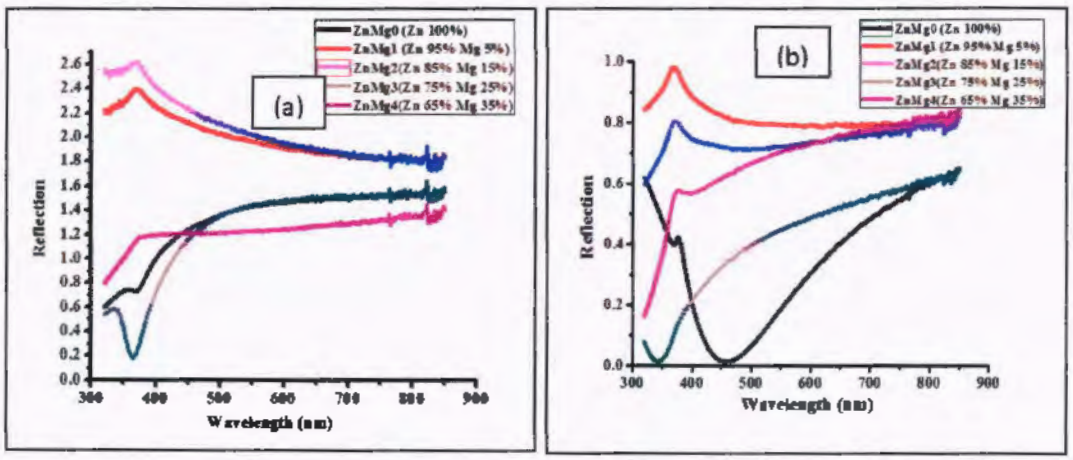

Fig 4.13: Reflection spectra of (a) unannealed and (b) annealed thin films.

Absorption:

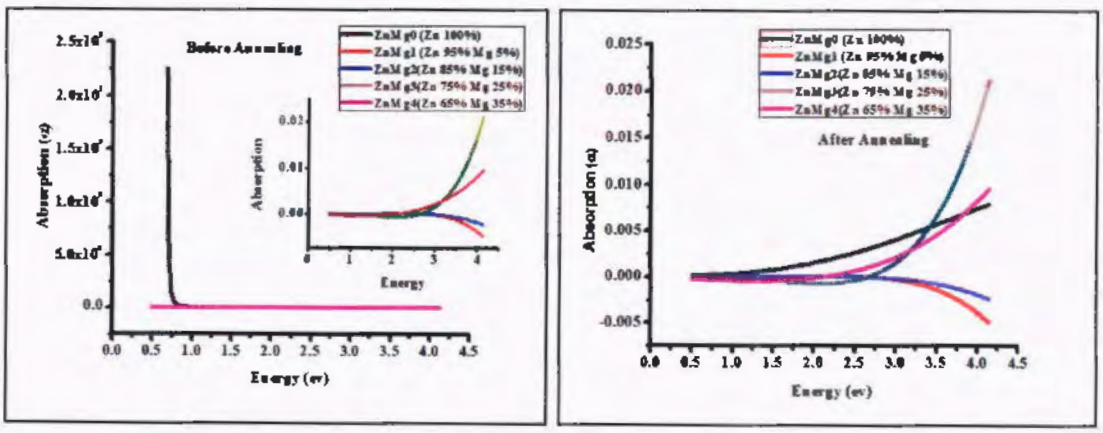

Fig 4.14: Absorption behavior of unannealed and annealed thin films.

Absorption behavior of as deposited and annealed thin films is shown in fig 4.14. It can be observed that ZnMg0 shows maximum absorption at 0.7 (IR range) in unannealed films which decreases to minimum value at 0.87 eV.

Absorption becomes negative in ZnMg1 and ZnMg2. Annealed thin films show similar behaviors as that of unannealed samples except ZnMg0 whose absorption shift from 1R to visible and UV range. ZnMg3 and ZnMg4 show maximum absorption in UV range where as ZnMg1 and ZnMg2 show negative absorption i.e. their behavior does not change with annealing.

Refractive Index:

Refractive index of unannealed and annealed thin films is shown in figure 4.15. Before annealing, thin film of ZnMg0 shows decrease in refractive index from 1.7 to 1.69 in wavelength range 300-350 nm then rapidly increases to maximum value gof refractive index i.e. 1.83 in figure 4.15 (before annealing). ZnMg2 and ZnMg4 show same behavior but different values of refractive index as deposited. Refractive index of ZnMg2 decreases slightly at 450 nm and then showed constant value. Refractive index of ZnMg4 rapidly decreased at 310 nm (in UV region) then quickly increased at 1.50, therefore shows no change in refractive index. ZnMg3 thin film shows maximum refractive index 1.73 in UV region then slowly moves down.

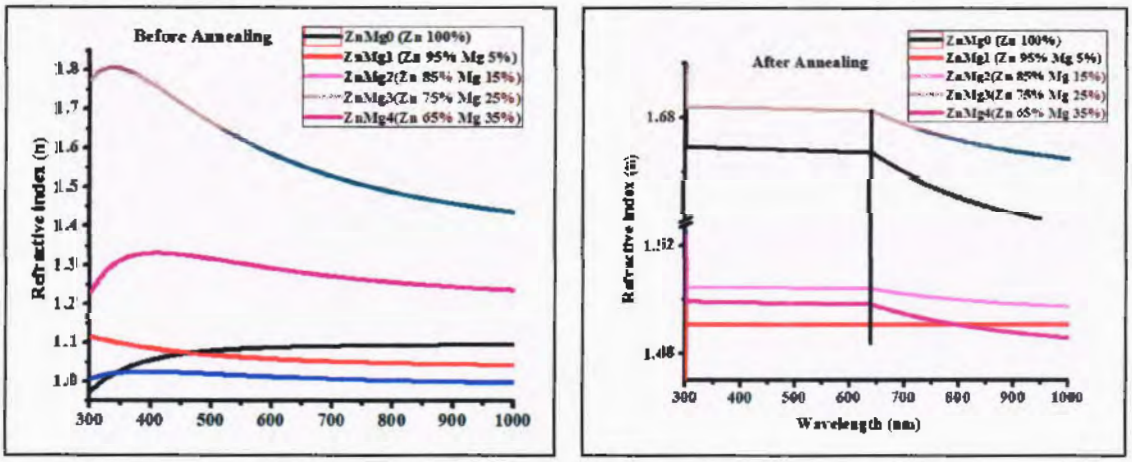

Fig 4.15: Refractive index of before and after annealing thin films.

After annealing, all samples show constant value of refractive index in orange region (400 to 640 nm) in figure 4.15 (after annealing). ZnMg2 shows same value of refractive index i.e. 1.49, which mean light does not pass through the sample at 600

nm. The refractive index in ZnMg3 decreased from 1.68 to 1.66 in wavelength range 650-1000 nm. ZnMg2, ZnMg0 and ZnMg4 show similar behavior like ZnMg3 but have different values of refractive index.

Extinction Coefficient K:

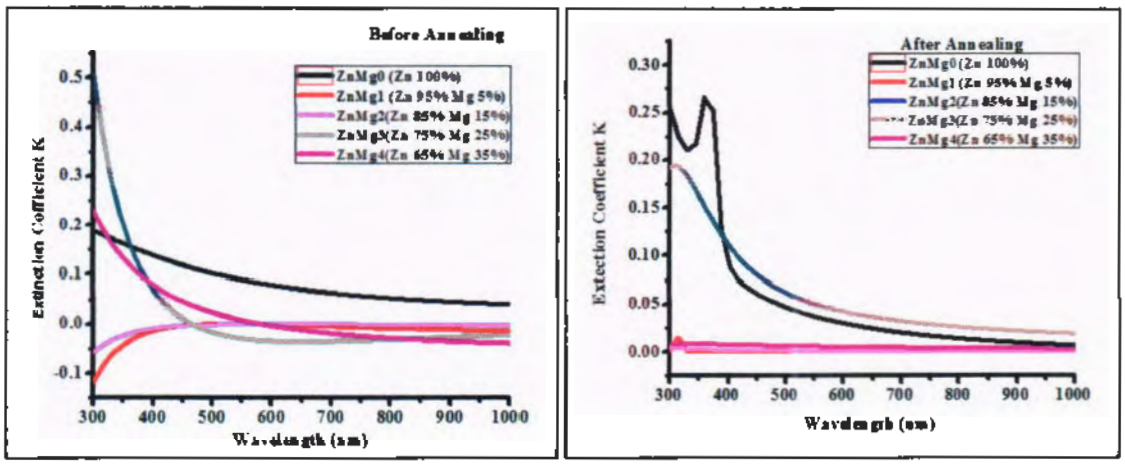

Fig 4.16: Extinction Coefficient of unannealed and annealed thin films.

Figure 4.16 shows relation of wavelength versus extinction coefficient for unannealed and annealed thin films. The extinction coefficient of ZnMg0, ZnMg3 and ZnMg4 increases in visible region and has no change in IR region as before annealing. It means, maximum light is absorbed in UV region and minimum in IR region. Before annealing, value of extinction coefficient decreases for ZnMg2 and ZnMg1 in UV region and has no change in visible and IR region.

After annealing, In case of ZnMg0, maximum value of extinction coefficient (k) appeared in UV region at 357 nm then decreased in visible region and IR region. ZnMg3 and ZnMg4 show no change in UV visible and IR regions. ZnMg2 show small value of K 0.01 at 312 nm in UV region then remain constant throughout the UV visible and IR region.

E1 Dielectric constant:

Dielectric constant of ZnMg3 is maximum at 3.29 in UV region then gradually decreases in visible and IR region in figure 4.17 (before annealing). ZnMg4 and ZnMg0 show similar behavior as ZnMg3 with different values of E1. In ZnMg1 and ZnMg2 values of E1 appear at 1.3 and 1.01 in UV region and remain constant in visible and NIR.

[46] E. Aperathitis, V. Kambilafka, M. Modreanu "*Properties of n-type Zn-N thin film as channel for transparent thin film transistors*" 2009 1036-1039.

[47] Jiang, N., et al., "Zinc nitride films prepared by reactive RF magnetron sputtering of zinc in nitrogen containing atmosphere". Journal of Physics D: Applied Physics, 2012.

[48] N. Yang, L Fan, J. Li, X. Wang, "Post annealing influence on property of N-In codoped ZnO thin film prepared by ion beam enhanced deposition method", **253** (2007) 4990-4993.

[49] H. Wang, X, Gao,Q. Duan, I. Lu, "Variation of surface properties of ZnO films by implantation of N ions", **492** (2005) 236-23.

[50] C. Wang, Z. Ji, K. Liu, Y. Xang, Z. Ye, "P-type ZnO thin films prepared by oxidation of Zn3N2 thin films deposited by DC magnetron sputtering", **259** (2003) 279-281.

nm. The refractive index in ZnMg3 decreased from 1.68 to 1.66 in wavelength range 650-1000 nm. ZnMg2, ZnMg0 and ZnMg4 show similar behavior like ZnMg3 but have different values of refractive index.

Extinction Coefficient K:

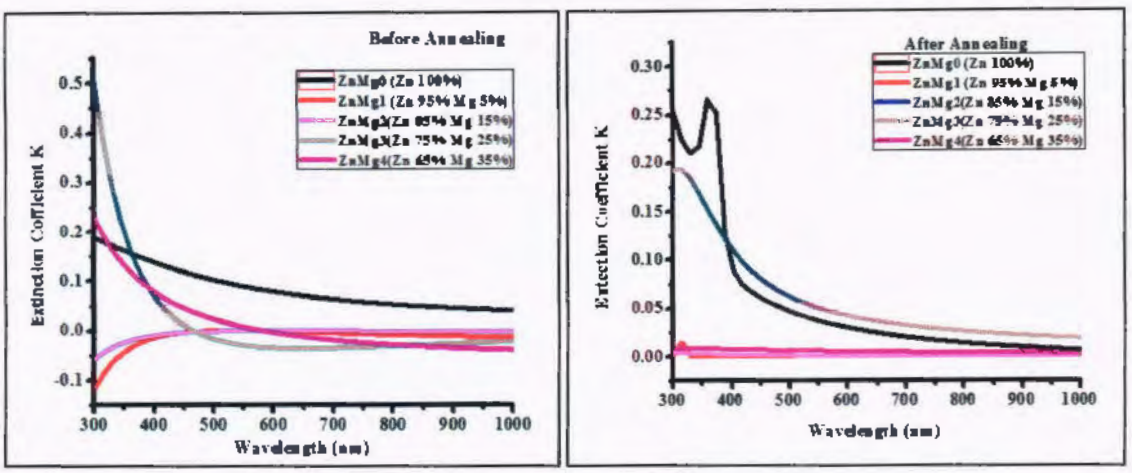

Fig 4.16: Extinction Coefficient of unannealed and annealed thin films.

Figure 4.16 shows relation of wavelength versus extinction coefficient for unannealed and annealed thin films. The extinction coefficient of ZnMg0, ZnMg3 and ZnMg4 increases in visible region and has no change in IR region as before annealing. It means, maximum light is absorbed in UV region and minimum in IR region. Before annealing, value of extinction coefficient decreases for ZnMg2 and ZnMg1 in UV region and has no change in visible and IR region.

After annealing, In case of ZnMg0, maximum value of extinction coefficient (k) appeared in UV region at 357 nm then decreased in visible region and IR region. ZnMg3 and ZnMg4 show no change in UV visible and IR regions. ZnMg2 show small value of K 0.01 at 312 nm in UV region then remain constant throughout the UV visible and IR region.

E1 Dielectric constant:

Dielectric constant of ZnMg3 is maximum at 3.29 in UV region then gradually decreases in visible and IR region in figure 4.17 (before annealing). ZnMg4 and ZnMg0 show similar behavior as ZnMg3 with different values of E1. In ZnMg1 and ZnMg2 values of E1 appear at 1.3 and 1.01 in UV region and remain constant in visible and NIR.

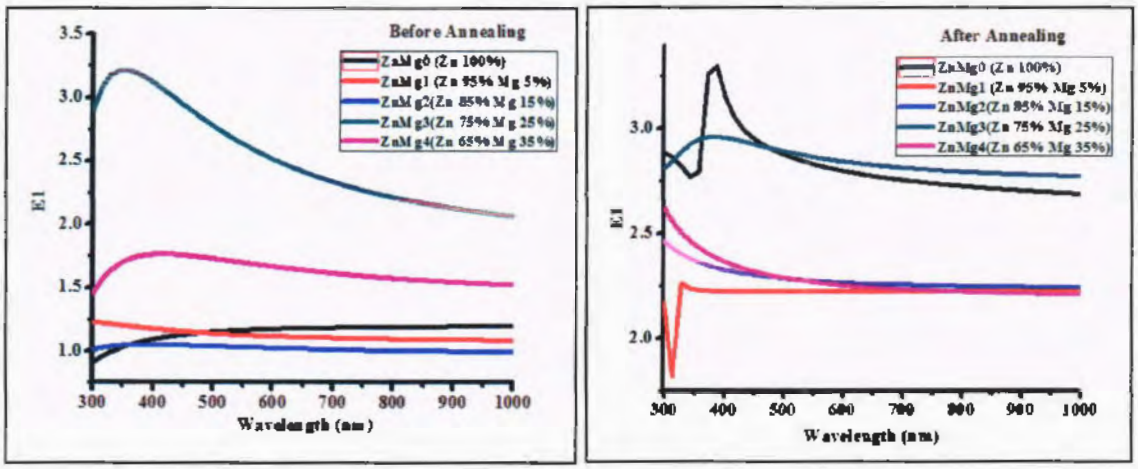

Fig 4.17: E_1 spectra of unannealed and annealed thin films.

After annealing, ZnMg0 shows maximum value of E1 at 3.3 in visible region and gradually decreases in visible and NIR region. ZnMg3 has E1 value 2.9 in UV region which slightly decreases in visible and NIR region. ZnMg2 and ZnMg4 have E1 values at 2.4 and 2.6 in UV region which remain constant after 500 nm in visible and NIR region.

E2 Dielectric loss:

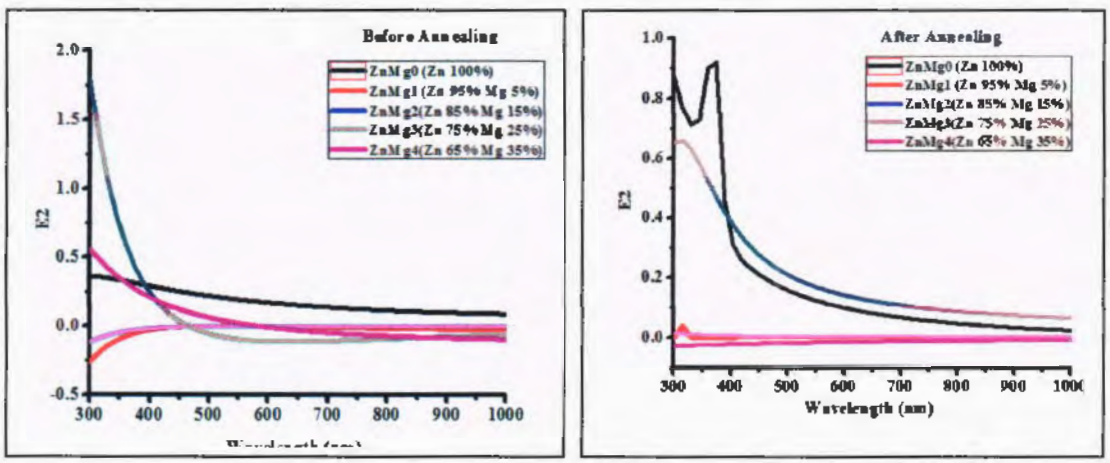

Fig 4.18: E_2 spectra of unannealed and annealed thin films.

ZnMg3 shows maximum value of E2 at 1.75 in UV region which sharply decreases in visible region and slightly increases in NIR region. ZnMg2 and ZnMg1 show negative value of E2 in UV region, and then slowly converted to positive value

in visible region and NIR. ZnMg0 slowly decreases in UV and visible region from 0.36 to 0.169. ZnMg4 has maximum value of E2 at 0.55 in 300 nm, after that it slowly decreased in visible and NIR region.

Figure 4.18 shows that the value of E2 for ZnMg0 is decreased i.e. 0.7 at 350 nm and then increased and reached to maximum value of 0.95 at 400 nm which then quickly decreased in UV region at after annealing. ZnMg3 has maximum value of E2 i.e. 0.67 which decreases in visible and NIR region. ZnMg2 has maximum value 0.01 of E2 in UV region which remains constant in visible and NIR region. ZnMg2 and ZnMg4 have no change in UV visible and NIR region.

Band gaps of thin films:

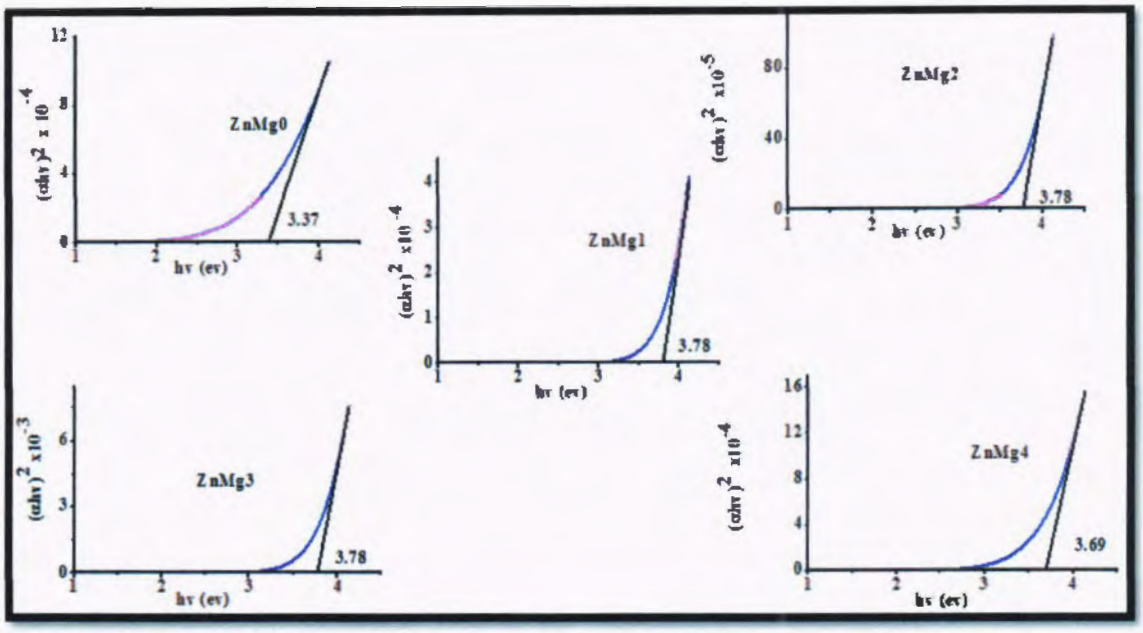

Fig 4.19: The graphs show the band gap of Zinc Magnesium nitride thin films before annealing.

Optical band gaps are calculated by the absorption spectra which show linear relation of $(\alpha hv)^2$ versus hv. Table no 5 shows slight difference in band gaps between UV-Visible and Ellipsometry. Band gap decreases after annealing due to increase of grain size and removed strain from thin films.

Table No 4.7: Comparison of band gap values of UV-Visible and SE.

Samples	UV-Visibe Reflection Band gap E_g (eV)		Ellipsometry Band gap E_g (eV)	
	Before Annealing	After Annealing	Before Annealing	After Annealing
Zn_3N_2 (Zn=100%)	1.76, 2.05	1.77	3.37	3.34
ZnMg1 (Zn=95%,Mg=5%)	1.79, 2.23	3.19	3.78	3.79
ZnMg2 (Zn=85%, Mg=15%)	1.73, 3.49	2.07, 3.21	3.78	3.74
ZnMg3 (Zn=75%, Mg=25%)	3.9	2.05	3.78	3.77
ZnMg4 (Zn=65%, Mg=35%)	1.79, 3.64	1.69	3.69	3.64

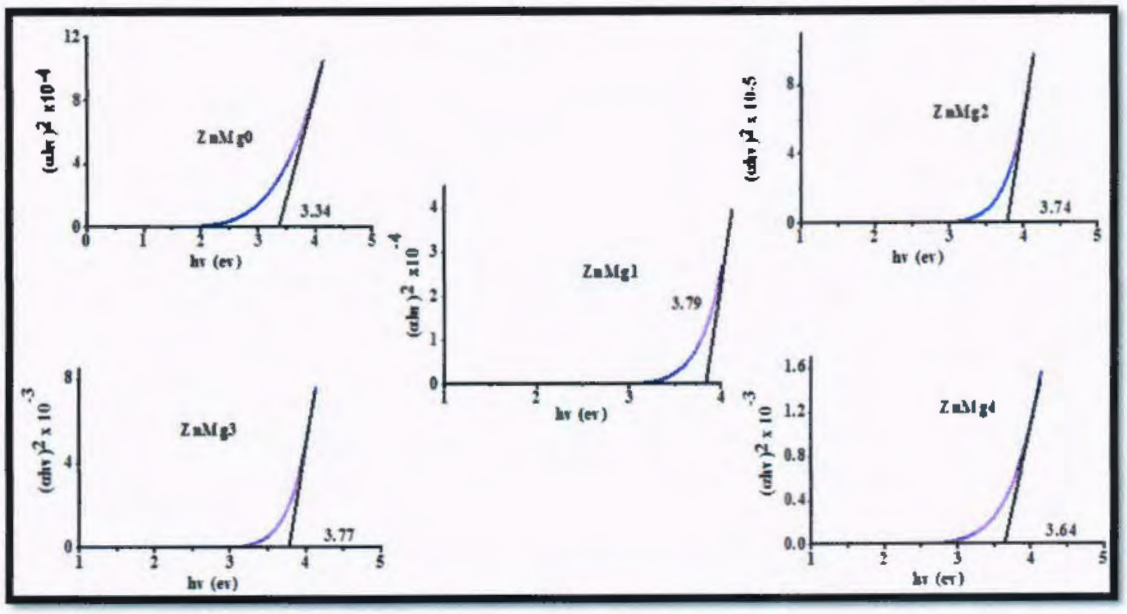

Fig 4.20: The graphs show the band gap of Zinc Magnesium nitride thin films after annealing.

In figures 4.19 and 4.20 all tauc plots showing decrease in band gaps after annealing, which are verified by UV-visible reflectance.

4.5.2 ZnMg thin films deposited on p-type silicon substrate:

Reflection Spectra:

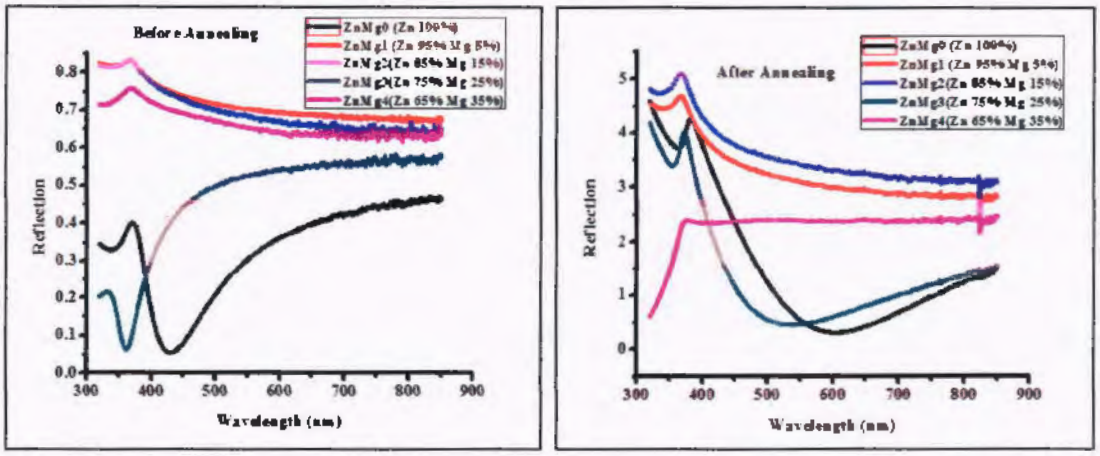

Fig 4.21: Reflection spectra of unannealed and annealed thin films.

Reflection spectra of unannealed thin films of ZnMg1 and ZnMg2 show maximum value at 0.83 in figure 4.21 (before annealing). ZnMg1, ZnMg2 and ZnMg4 show same behavior but different values of reflection. ZnMg0 has maximum value of reflection i.e. 0.4 at 350 nm. After that it decreases sharply within wavelength range 350-410 nm and then gradually increases between 410-800 nm.

After Annealing (figure 4.17 after annealing), ZnMg2 and ZnMg1 have similar behaviors like unannealed thin films with high value of reflection. ZnMg4 has maximum value of reflection i.e. 2.2 in UV region at 356 nm after that it has no change in visible region. ZnMg3 and ZnMg4 show two maximum value of reflection 4.5 and 4.3 at 320 and 400nm. There move slowly downward at 600nm then move upward gradually at 800 nm.

Absorption:

Before annealing, ZnMg1 shows absorption 0.32 at 3.5 eV. The absorption of light in remaining samples has very low in figure 4.22.

After annealing, ZnMg0 showed maximum absorption value 2.3×10^{9} at 0.7 eV which then decreased at 0.87eV and ZnMg1 shows change in absorption at 3.6ev

and randomly increase at 0.0005. ZnMg2, ZnMg3 and ZnMg4 show similar behavior of absorption with different values.

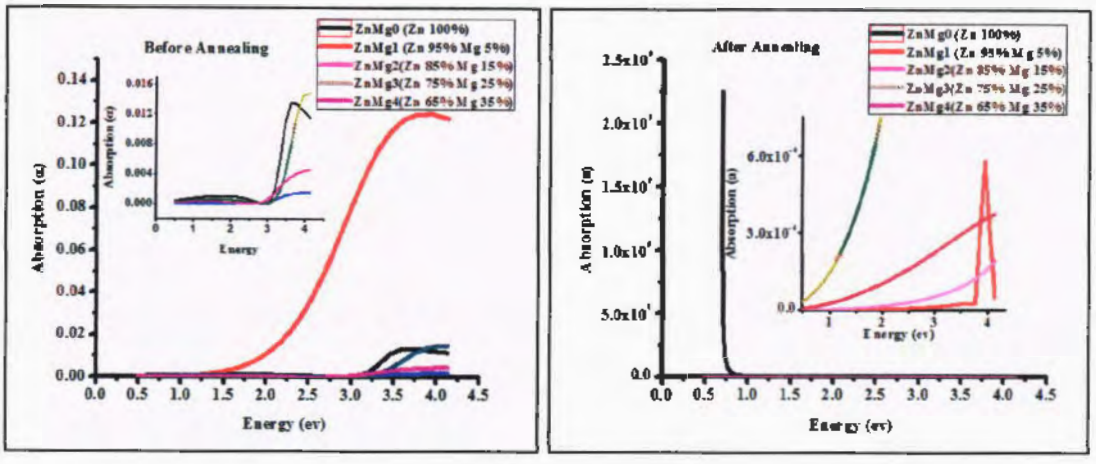

Fig 4.22: Absorption behavior of unannealed and annealed thin films.

Refractive Index:

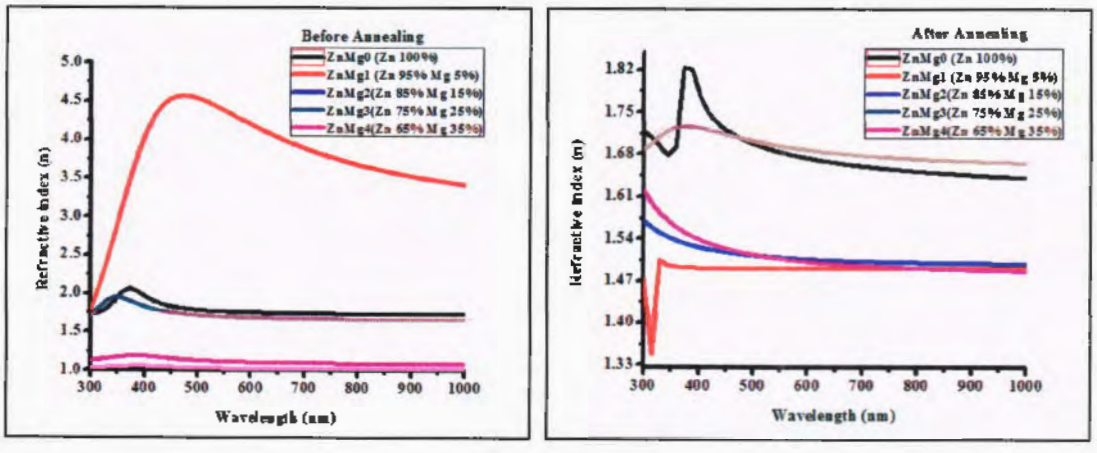

Fig 4.23: Refractive index of annealed and unannealed thin films.

All samples in fig 4.23 have similar behavior which firstly increases steadily and then slowly decreases with different values of refractive index at before annealing.

After annealing, ZnMg0 has maximum value of refractive index i.e. 1.34 which decreases in visible and NIR region. ZnMg1 shows opposite behavior to ZnMg0 i.e. it shows gradual decrease in refractive index 1.50 and 1.66 in UV region and remains constant in visible.

Extinction Coefficient (k):

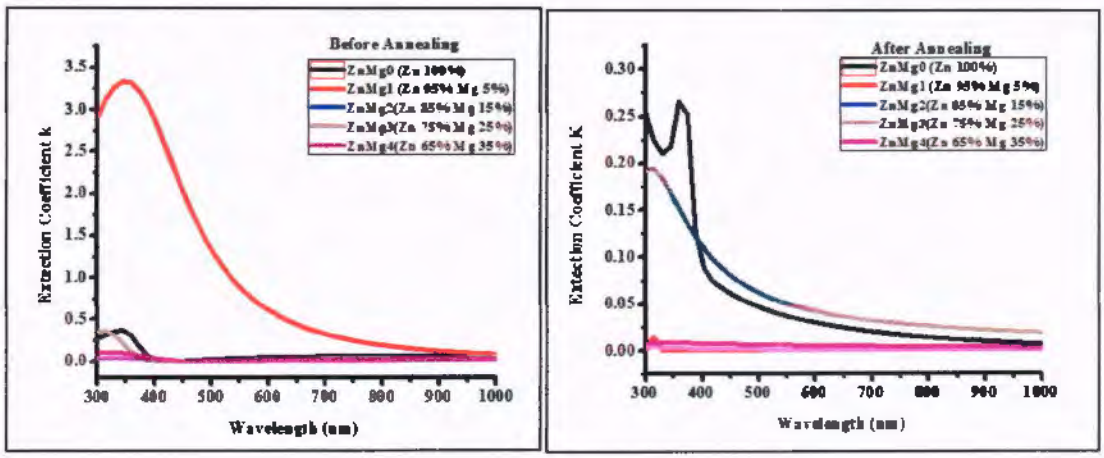

Fig 4.24: Extinction Coefficient of unannealed and annealed thin films.

Before annealing ZnMg1 shows maximum value of 3.48 in visible region and decreases in NIR region. Remaining samples show small fluctuation in UV region and no change in visible and NIR in figure no 4.24.

After annealing, ZnMg0 and ZnMg3 show maximum value of k at 0.25 and 0.19 in visible region. ZnMg1, ZnMg2 and ZnMg4 have shown very small values of (k).

E1 Dielectric Constant:

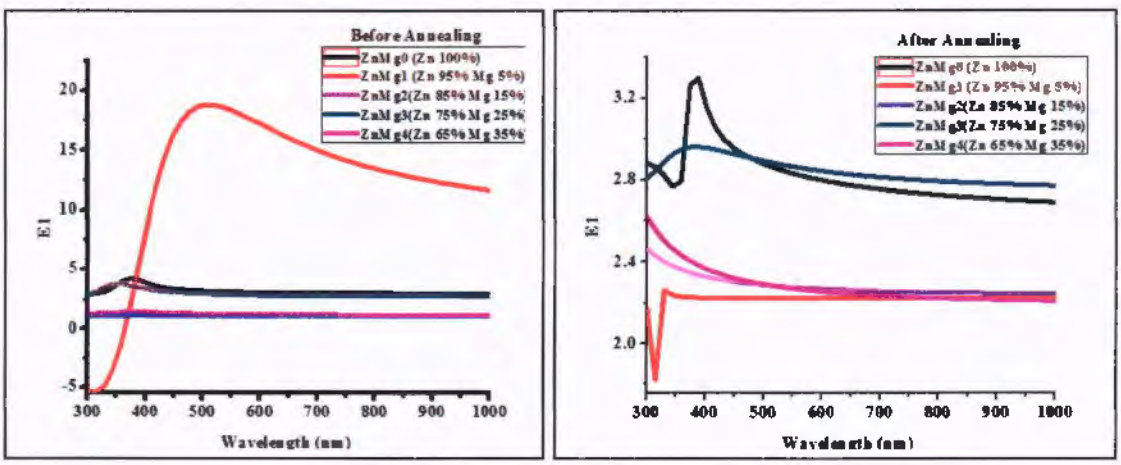

Fig 4.25: E_1 spectra of unannealed and annealed thin films.

Before annealing, Dielectric constant is maximum in ZnMg1 in UV region and steadily decreases in IR region. Dielectric constant in ZnMg0 and ZnMg3 also slightly increases in UV region and remain constant in IR region. In ZnMg2 and ZnMg4 the dielectric constant remains same at 3 throughout all regions.

After annealing, $ZnMg_0$ and ZnMg3 have maximum dielectric constant values 3.3 and 3.0 which decrease slowly in visible and NIR region. ZnMg1 shows opposite behavior to that of ZnMg0. ZnMg2 and ZnMg4 show gradual decrease in E1 values i.e. 2.6 and 2.5 respectively in UV region and remain constant in visible region (figure 4.25 After annealing).

E2 Dielectric loss:

Before annealing ZnMg1 shows maximum value of 24 at 450 nm in visible region which decreases further. Remaining samples show small fluctuation in UV region and has slightly change in visible and NIR as shown in figure 4.26 (before annealing).

After annealing, ZnMg0 and ZnMg3 show maximum value of E2 at 0.9 and 0.7 respectively in visible region. ZnMg1, ZnMg2 and ZnMg4 have shown very small values of dielectric constant.

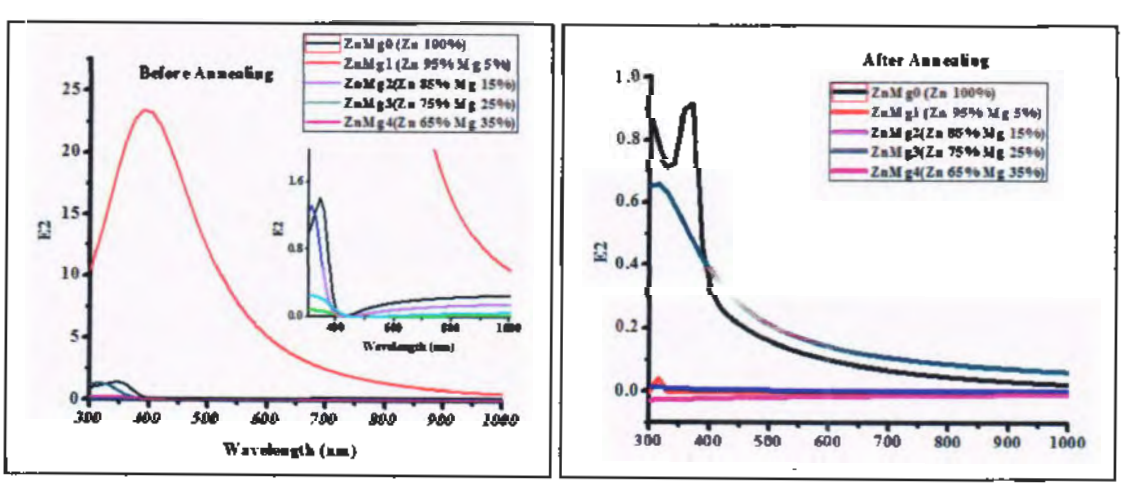

Fig 4.26: E_2 spectra of unannealed and annealed thin films.

Band gap of thin films:

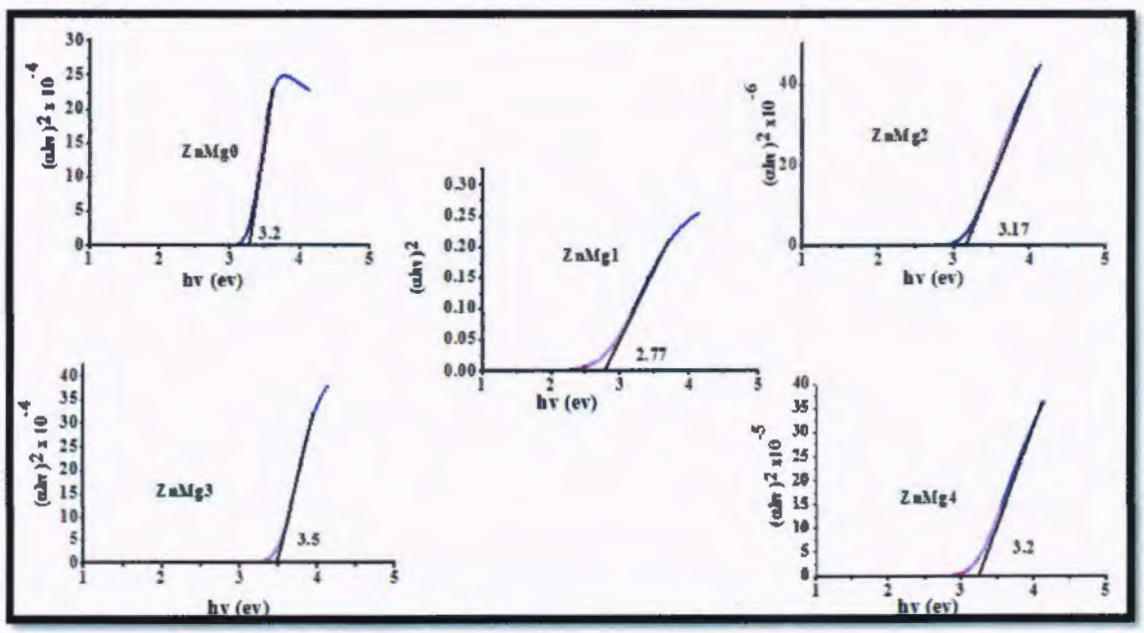

Fig 4.27: The band gap of Zinc Magnesium nitride thin films (before annealing).

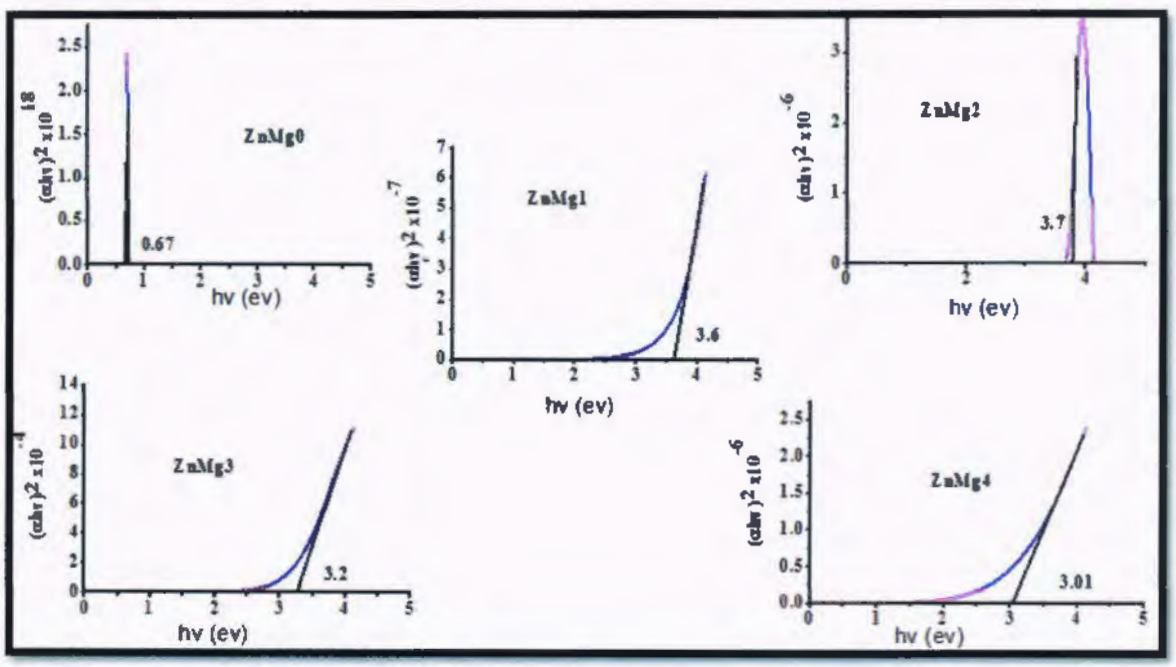

Fig 4.28: The band gap of Zinc Magnesium nitride thin films (after annealing).

In figures 4.27 and 4.28 all tauc plots showing decrease in band gaps after annealing, which are verified by UV-visible reflectance.

Table No 4.8: Comparison of band gap values of UV-Visible and SE.

Samples	UV-Visible Reflection E_g (eV)		Ellipsometry E_g (eV)	
	Before Annealing	After Annealing	Before Annealing	After Annealing
Zn_3N_2 (Zn=100%)	2.46	1.51	3.2	0.67
ZnMg1(Zn=95%, Mg=5%)	3.5, 4.5	3.27, 3.59	2.77	3.6
ZnMg2(Zn=85%, Mg=15%)	3.48, 4.3, 4.6	1.89, 3.14	3.17	3.7
ZnMg3(Zn=75%, Mg=25%)	2.5, 3.54	1.64	3.5	3.2
ZnMg4(Zn=65%, Mg=35%)	3.3, 3.9, 4.4	1.8, 2.3, 3.29	3.2	3.01

Optical band gaps are calculated by the absorption spectra which show linear relation of $(\alpha h\nu)^2$ versus hv. Table no 5 shows slight difference in band gaps between UV-Visible and Ellipsometry. Band gap decreases after annealing due to increase of grain size and strain is removed from thin films.

4.6 Electrical Properties:

4.6.1 ZnMg thin film deposited on p-type silicon substrate:

Hall Effect measurements were carried out for the calculations of the mobility, conductivity, sheet resistance and carrier concentration. The amount of magnetic field used was 0.5 Tesla. Hall measurements were repeated several times for eacb sample to ensure the consistency of results. The thin film was converted from n-type to p-type after annealing in table 4.13.

With an increase in oxidation temperature, more and more nitrogen acceptors ZnO:N were activated and they rewarded more and more electrons produced by intrinsic defects in the ZnO:N thin films. Therefore, the carrier density of holes is increased as reported earlier [45].

Table 4.9: Electrical properties calculated by Hall Measurements

Samples	Sheet Resistance	Surface Carrier density	Volume Carrier density	Mobility	Conductivity	Types
Before Annealing						
ZnMg0	205056.46	-4.20137×10^{14}	2.64×10^{20}	0.07874	0.657	N
ZnMg1	1.049×10^{6}	-1.04499×10^{15}	1.193×10^{20}	0.0671	0.117	N
ZnMg2	547083.67	-1.03534×10^{15}	1.193×10^{20}	0.03555	0.372	N
ZnMg3	659923.67	-4.68893×10^{15}	2.74×10^{20}	0.00547	0.301	N
ZnMg4	1.050×10^{6}	-1.69459×10^{15}	1.11×10^{21}	0.00643	0.189	N
After Annealing						
ZnMg0	1.40×10^{4}	1.93×10^{12}	1.78×10^{17}	4.69×10^{2}	7.10	P
ZnMg1	1.22×10^{5}	7.46×10^{11}	2.03×10^{17}	2.43×10^{2}	2.30	P
ZnMg2	2.09×10^{4}	3.41×10^{11}	9.16×10^{16}	1.48×10^{3}	13	P
ZnMg3	7.83×10^{4}	1.64×10^{11}	1.71×10^{16}	1.26×10^{3}	4.45	P
ZnMg4	8.64×10^{3}	2.03×10^{13}	3.72×10^{18}	5.38×10^{2}	22.6	P

4.6.1.2 Mobility:

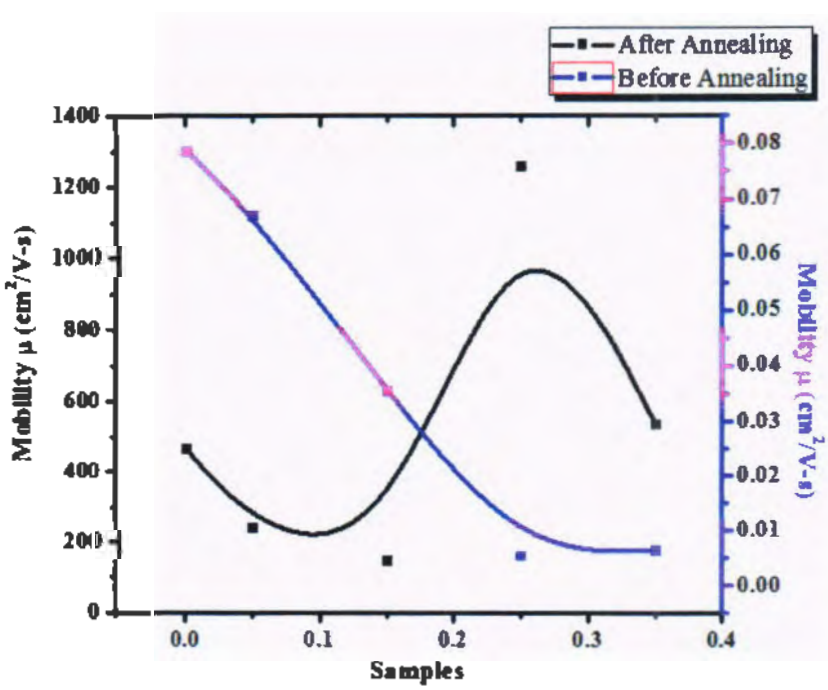

Fig 4.29: Mobility of samples before and after annealing.

Before Annealing, mobility was linearly decreased from samples ZnMg0 to ZnMg3. It increases in ZnMg4 due to increased concentration of magnesium. After annealing, mobility of ZnMg0 to ZnMg4 increases as compared to before annealing i.e. 449 cm^2/V-s due to removed tensile strain from thin films which is also evident from XRD results. At higher temperature, the electrical properties of films deteriorated, while mobility increases as observed [46].

4.6.1.2 Carrier Concentration:

After Annealing, carrier concentration decreases as compared to pre-annealing in figure 4.30 [46]. Carrier concentration of samples increases from ZnMg2 to ZnMg4 before annealing. Mobility of thin films is increasing with decreasing carrier concentration which indicates that grain boundary is dominant [47].

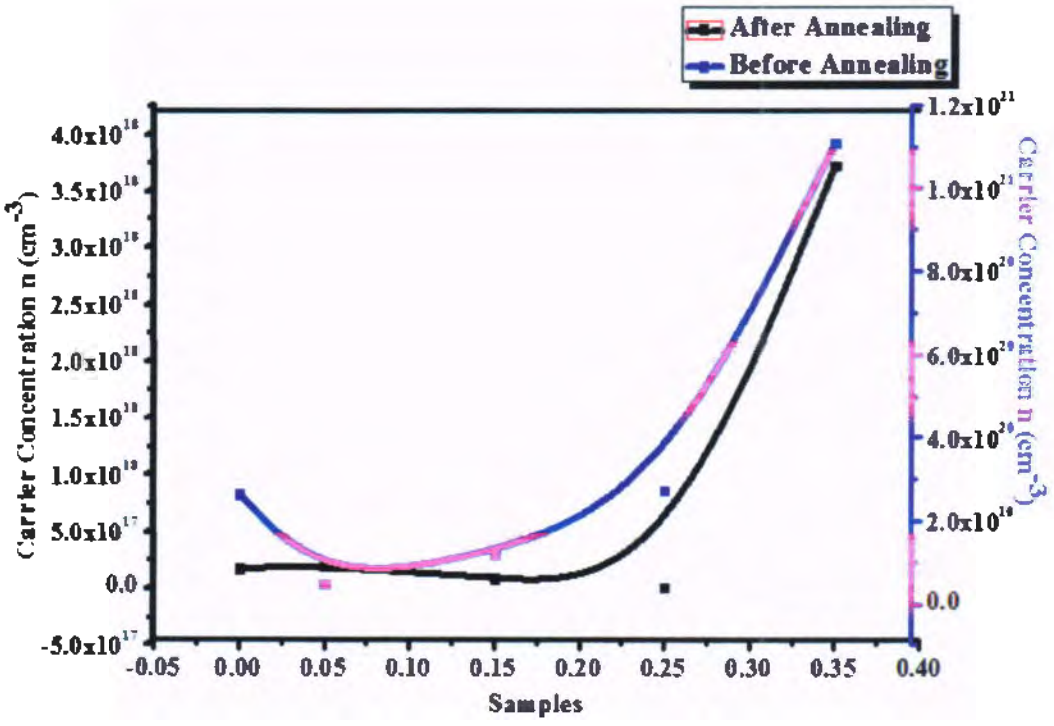

Fig 4.30: Carrier Concentration of samples before and after annealing.

4.6.1.3 Sheet Resistance:

In figure 4.31 shows that sheet resistance of samples decreased after annealing due to increased mobility. Before Annealing, sheet resistance was increased from ZnMg0 to ZnMg1 and drastically decreased to ZnMg2. Then again sheet resistance was increased for ZnMg3 and decreased for ZnMg4. Sheet resistance of ZnMg4 is

found to be increasing after annealing due to exclusion of defects. The XRD of ZnMg4 also showed the homogenous behavior.

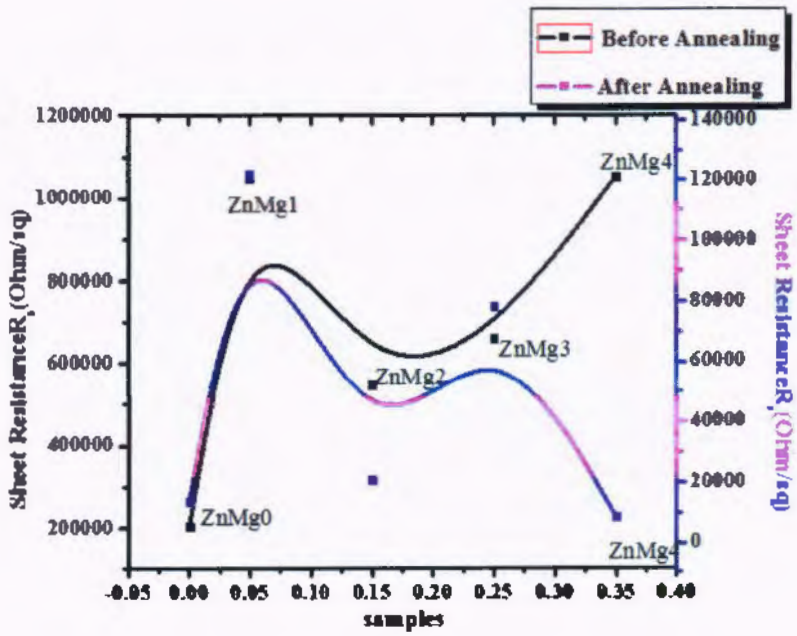

Fig 4.31: Sheet resistance of samples before and after annealing.

4.6.1.4 IV Curves:

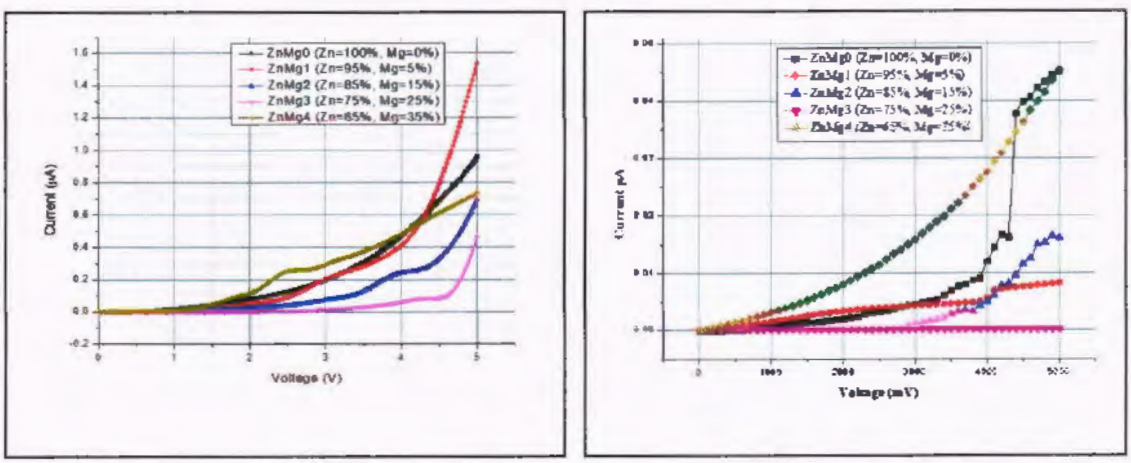

Fig 4.32: IV curves of samples before annealing

The IV curves show semiconductor behavior of films. After annealing, the current of samples is reduced as contrast to before annealing and films changed from n-type to p-type. By Hall measurements, it is cleared that electron concentration is

reduced and holes concentration is increased. Thin film rearranges itself and improved crystallinity at 800 ^{0}C. When electrical filed is applied, the holes and electrons recombine and make pairs due to which holes left in less quantity so current decreases after annealing.

4.6.2 Thin film deposited on n-type silicon substrate:

The Electrical properties of samples that are calculated by Hall measurements are given in table 4.14.The current of ZnMg0 was out of range of machine used for carrying out these electrical characterizations. By increasing oxidizing temperature, the Zn-N bonds break down and some nitrogen escaped from interstitial sites in thin films and this process led to an increase in the intrinsic defects which act as donors [49]. The concentration of holes is less and density of intrinsic defects becomes dominant so conduction changed from p-type to n-type [48, 49]. The range of current of pure zinc nitride thin films is found to be lying beyond the used apparatus limits.

Table 4.10: The Electrical Properties calculated by Hall Measurements.

Samples	Sheet resistance	Surface carrier density	Volume carrier density	Mobility	Conductivity	Types
Before Annealing						
ZnMg0	1.22×10^{5}	-5.65×10^{12}	-3.64×10^{12}	28.3	0.526	N
ZnMg1	8.62×10^{5}	5.88×10^{10}	8.01×10^{5}	256	0.258	P
ZnMg2	1.63×10^{5}	7.65×10^{11}	5.40×10^{10}	469	0.447	P
ZnMg3	3.34×10^{5}	5.39×10^{11}	9.71×10^{16}	167	0.704	P
ZnMg4	6.83×10^{5}	1.86×10^{11}	2.82×10^{10}	71	0.223	P
After Annealing						
ZnMg0						
ZnMg1	1.56×10^{6}	-8.45×10^{10}	-2.81×10^{16}	131	0.218	N
ZnMg2	1.41×10^{5}	-4.87×10^{11}	-1.04×10^{17}	264	1.53	N
ZnMg3	1.51×10^{6}	-5.61×10^{10}	-8.28×10^{15}	205	980	N
ZnMg4	2.30×10^{6}	-4.36×10^{10}	-3.41×10^{15}	72.9	826	N

4.6.2.1 Mobility:

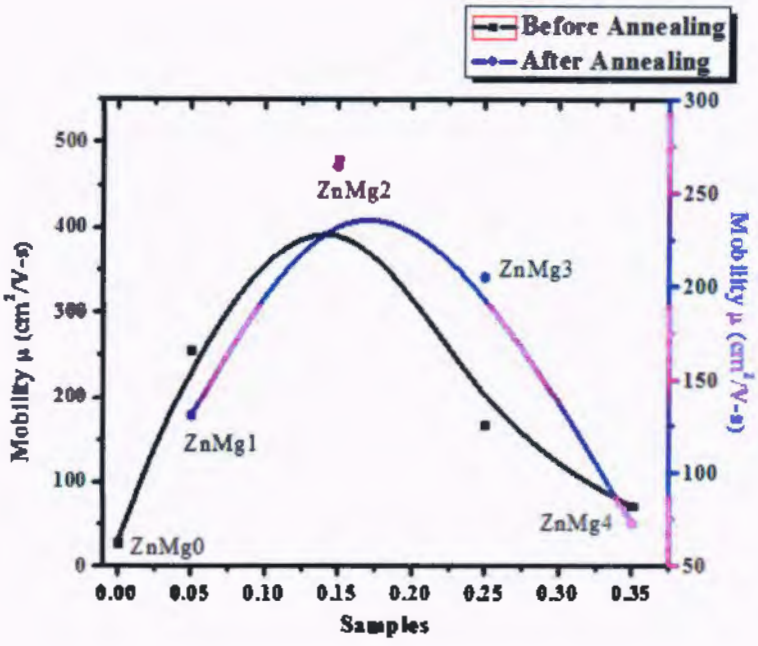

Fig 4.33: Mobility of samples before and after annealing.

The scattering of holes is due to the ionization of nitrogen acceptors that are responsible for decrease in mobility [50]. After annealing, the atoms/molecules in the thin films make stronger bond with each other and strain and defects are removed so that mobility of thin film decreases in figure 4.33 [50].

4.6.2.1 Carrier Concentration:

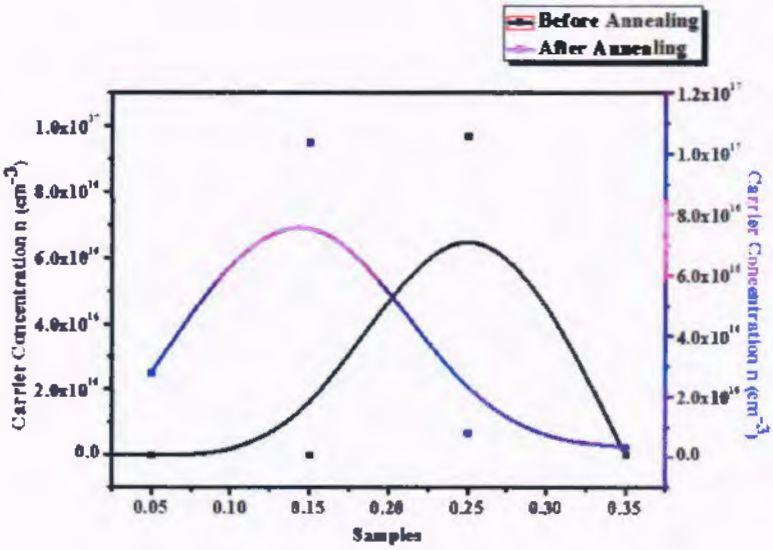

Fig 4.34: Carrier Concentration of samples before and after annealing.

Carrier concentration is increased in pre-annealing stage due to defects and vacancies. After annealing, almost all the defects and strains are reduced which is confirmed by XRD and PL results. So carrier concentration decreases after annealing.

4.6.2.3 IV curves:

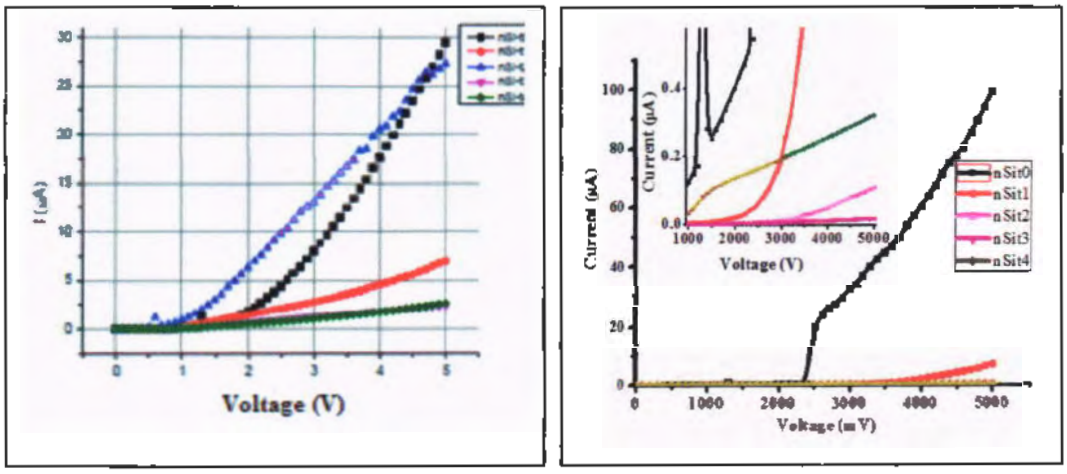

Fig 4.35: IV curves of thin film before and after Annealing.

The IV curves of the samples show the Ohmic behavior. The IV curve of ZnMg0 is higher as compared to other samples for after and before annealing due to maximum absorption of light and heat loses that is confirmed by Ellipsometry results. The current is decreasing for ZnMg1 to ZnMg4 after annealing due to a minimum absorption of light and Extinction Coefficient.

Conclusion

- The grain size of particles increased and stress are decreased in thin film through annealing.
- Increase in particle size in film due to annealing resulted in decrease in the band gap.
- Raman analysis exhibit that oxygen is incorporated in films and Nitrogen bonded to zinc has been replaced by Oxygen.
- Defects in films are mostly removed from film which is clear by the suppression of many photoluminescence transitions in annealed samples.
- Mobility of film increase and carrier concentration decrease of film after annealing which shows that defect in the films were acting as trap centers for charges.

References

[1] H. Juza, and Z. Hahn , Anorg. Allg Chem., 224 (1940) 25.

[2] N. Jiang, D.G. Georgiev, T. Wen, A.H. Jayatissa, "Crucial role of reactive pulse-gas on a sputtered Zn_3N_2 thin film formation" Thin Solid Films 520 (2012) 1698–1704.

[3] E. Maile, R.A. Fischer, Chemical Vapor Deposition 11 (2005) 409–414.

[4] K.toyoura, H.Tsyoura, H.Tsujimura, T.Goto, K.Hachiya, R.Hagineara, Y.Ito, Thin solid films 492, 88(2005).

[5] F.Zong, H,Ma, W.Du, J.Ma, X.Zhang, H.Xiao, F.Ji, C.Xue "Impact of air exposure on the chemieal and electronic structure of $ZnO:Zn_3N_2$ thin films" Appl.Surf Sci. 252, 7983 (2006).

[6] Melo, M.L.L.M.S.d., "*Deposition of Zn3N2 thin films and application in TFT structures*", in *Physics Dept.* 2014, ist: Lisbon, Portugal.

[7] Suda, T. and K. Kakishita, "*Band-gap energy and electron effective mass of polycrystalline Zn3N2*". Journal of Applied Physics, 2006. 99(7): p. 076101.

[8] Jiang, N., D.G. Georgiev, and A.H. Jayatissa, "*The effects of the pressure and the oxygen content of the sputtering gas on the structure and the properties of zinc oxy-nitride thin films deposited by reactive sputtering of zinc*". Semiconductor Science and Technology, 2013. 28: p. 025009.

[9] Kambilafka, V., et al., "*Thermal oxidation of n-type ZnN films made by rf-sputtering from a zinc nitride target, and their conversion into p-type films. Superlattices and Microstructures*", 2007. 42: p. 55-61.

[10] *static.ifp.tuwien.ac.at/homepages/Personen/Thin film technology/Physics of thin films.*

[11] Ting Wen, Madhav Gautam, Amir M. Soleimanpour, Ahalapitiya H. Jayatissa "*Thermal annealing effect on zinc nitride thin films depositedby reactive rf-magnetron sputtering process*" 16 (2013) 318-325.

[12] Xue Cs, AiYJ, Sun LL (2007) "*Synthesis and photoluminescence properties of Mg3N2 powders Rare Met Matter Eng*" 36; 2020-2022.

[13] Murata T, Itatani K, Howell FS, Kishioka A, Kinoshita.M (1993) "*preparation of magnesium nitride powder by low-pressure chemical vapor deposition*", Jam Ceram. Soc. 76:2909-2911.

[14] Toyoura K, Goto T, Hagiwara R (2005) "*structural and optical properties of Mg3N2 formed by a novel electrochemical process Electrochim Acta*" 51: 56-60

[15] Armenta MGM, Rayes-Serrato A, Borja MA (2000) "*Ab initio determination of the electronic structure of beryllium-aluminum and Magnesium-nitrides, A Comparative study*", phy Rev B 62: 4890.

[16] H.Lorenz, I.Orgzall, Diam, Relat.Matter. 4(1995) 1046.

[17] Sidra Shakoor "*Fabrication and characterization of* $(Zn_{1-x}Mg_x)_3N_2$ *thin films with different compositions*" 2015 IIUI.

[18] P.J Kelly and R.D Arnell, "*Magnetron sputtering: a review of recent developments and applications*", vacuum, vol.56, no 3, Pp. 159-172, 2000.

[19] J. Seller, "Asymmetric bipolar pulsed DC the enabling technology for reactive PVD, surface and coatings Technology", **98**, no 1-3 pp, 1245-1250, 1998.

[20] Harris, D.C,Bertolucci MD, symmetrety and spectroscopy : *an introduction to vibrational and electronic spectroscopy.*

[21] Raman Spectroscopy Umesh P. Agarwal and Rajai H. Atalla USDA Forest Products Laboratory, Madison, Wisconsin, U.S.A."Raman Spectroscopy" chap 8 (1995).

[22] SPECTROSCOPIC ELLIPSOMETRY* ROVENA PASCU, MARIA DINESCU National Institute for Laser, Plasma and Radiation Physics Atomistilor Str., No. 409, PO Box MG-16, 077125, Magurele, Bucharest, Romania E-mail: rovena.pascu@inflpr.ro, dinescum@ilin.nipne.ro Received July 12, 2010.

[23] Jiang, N., et al., "Zinc nitride films prepared by reactive RF magnetron sputtering of zinc in nitrogen containing atmosphere". Journal of Physics D: Applied Physics, 2012.

[24] Sharma, S., et al., "Structural and optical characterization of ZnO thin films for optoelectronic deVice application by RF sputtering technique". Supperlattices and Microstructure, 2014.

[25] V. Kambilafka, P. Voulgaropoulou, S. Dounis, E. Iliopoulos, M. Androulidaki, K. Tsagaraki, V. Saly, M. Ruzinsky, P. Prokein, E. Aperathitis, "Green photoluminescence from Zn_3N_2:Tb films prepared by magnetron sputtering" Thin Solid Films 515 (2007) 8573.

[26] P. Kumbhakar*, D. Singh, C. S. Tiwary, and A. K. Mitra "*Chemical synthesis and visible photoluminimumescence emission from monodispersed zno nanoparticles*" Chalcogenide Letters 5, No. 12, December 2008, p. 387 – 394.

[27] Xuesi Qin, Guojian Li, Lin Xiao, Guozhen Chen, Kai Wang, and Qiang Wang "Effect of Oxidation Condition on Growth of N: ZnO Prepared by Oxidizing Sputtering Zn-N Films" **11** (2016).

[28] N.H. Erdogan, K, Kara, H. Ozdamar, R. Esen, H. Kavak "Effect of the oxidation temperature on microstructure and conductivity of ZnxNy thin films and their conversion into p-type ZnO:N films" Applied Surface Science **271** (2013) 70-76.

[29] S. Han , J. Zhang, Z. Zhang, Y. Zhao, L. Wang, J. Zheng, B. Yao, D. Zhao, D. Shen, "$Mg_{0.58}Zn_{0.42}O$ thin films on MgO subtrates with MgO buffer layer". Appl. Mater. Interfaces 2(7), 1918-1921 (2010).

[31] K. A. Alim, V. A. Fonoberov, M. Shamsa, A. A. Ba- landin, "Micro-Raman investigation of optical phonons in ZnO nanocrystals" J. Appl. Phys. 97, 124313 (2005).

[32] S. B. Yahia, L. Znaidi, A. KanaeV, J. P. Petitet, "Raman study of oriented ZnO thin films deposited by sol-gel method" 1234 (2008).

[33] D. L. Golic, G. Brankovic, M. P. Nesic, K. Vojisavlje- vic, A. Recnik, N. Daneu, S. Bernik, M. Scepanovic, D. Poleti, Z. Brankovic, Nanotechnology 22, 395603 (2011).

[34] Xing, G. Z., et al., "Structural and electrical characterization of high quality (100) oriented- Zn_3N_2 thin films grown by radio-frequency magnetron sputtering" Journal of Applied Physics, 2010. 108.

[35] GeorgieV, D.G., et at., "Microstructure and Electronic properties of Zinc Nitride Thin films, in Nanotechnology Materials and Device Conference". 2009: Traverse City, Michigan,USA.

[36] C.Wang .Z.Ji, K. Liu, Y.Xiang,Z.Ye, "P-type ZnO thin films prepared by oxidation Of Zn3N2 thin films deposited by DC magnetron sputtering", Journal of Crystal Growth **259** (2003) 279-281.

[37] X.C Wang, W.B. Mi, S. Dong X.M. Chen, B.H. Yang , "Microstructure and optical property of N-incorporated polycrystalline ZnO films", Journal of alloys and compound **478** (2009) 3544-3547.

[38] Soumen Dhara, P.K. Giri "stable p-type conductivity and enhanced photoconductivity from nitrogen doped annealed ZnO thin films" **520** (2012) 5000-5006. Pl.

[39] K. Vanheusden, W.L. Warren, C.H. Seager, D.K. Tallant, J.A. Voigt, B.E. Gnade, "Photoluminescence of Zinc Oxide Nanowires: The Effect of Surface Band Bending " J. Appl. Phys. **79** (1996) 7983.

[40] P. K. Giri, S. Bhattacharyya, D. K. Singh, R. Kesavamoorthy, B. K. Panigrahi, K. G. M. Nair, "High temperature ferromagnetism and optical properties of Co doped ZnO nanoparticles" J. Appl. Phys. **102** (2007) 093515.

[41] Ren-Yu Tian, Yu-Jun Zhao, The origin of p-type conduction in (P, N) codoped ZnO J. Appl. Phys. **106** (2009) 043707-1-6.

[42] N. C. S. Selvam, R. T. Kumar, L. J. Kennedy, and J. J. Vijaya, "Comparative study of microwave and conventional methods for the preparation and optical properties of novel MgO-micro and nano-structures," *Journal of Alloys and Compounds*, **509**, (2011) no. 41, pp. 9809–9815.

[43] Y. Hao, G. Meng, C. Ye, X. Zhang, and L. Zhang, "Kinetics driven growth of orthogonally branched single-crystalline magnesium oxide nanostructures," *Journal of Physical Chemistry B*, **109**, (2005) 11204–11208 .

[45] B. S. Li, Y. C. Liu, Z. Z. Zhi, D. Z. Shen, Y. M. Lu, I. Y. Zhang, X. W. Fan, R. X. Mu, D .O. "Henderson, optical properties and electrical characterization of p-type ZnO thin films prepared by thermally oxidizing Zn_3N_2 thin films", Journal of Materials Research **18** (2003) 8-17.

[46] E. Aperathitis, V. Kambilafka, M. Modreanu "*Properties of n-type Zn-N thin film as channel for transparent thin film transistors*" 2009 1036-1039.

[47] Jiang, N., et al., "Zinc nitride films prepared by reactive RF magnetron sputtering of zinc in nitrogen containing atmosphere". Journal of Physics D: Applied Physics, 2012.

[48] N. Yang, L Fan, J. Li, X. Wang, "Post annealing influence on property of N-In codoped ZnO thin film prepared by ion beam enhanced deposition method", **253** (2007) 4990-4993.

[49] H. Wang, X, Gao,Q. Duan, I. Lu, "Variation of surface properties of ZnO films by implantation of N ions", **492** (2005) 236-23.

[50] C. Wang, Z. Ji, K. Liu, Y. Xang, Z. Ye, "P-type ZnO thin films prepared by oxidation of Zn3N2 thin films deposited by DC magnetron sputtering", **259** (2003) 279-281.